

Adversarial Training is a Form of Data-dependent Operator Norm Regularization

Kevin Roth^{*1} Yannic Kilcher^{*1} Thomas Hofmann¹

Abstract

We establish a theoretical link between adversarial training and operator norm regularization for deep neural networks. Specifically, we prove that ℓ_p -norm constrained projected gradient ascent based adversarial training with an ℓ_q -norm loss on the logits of clean and perturbed inputs is equivalent to data-dependent (p, q) operator norm regularization. This fundamental connection confirms the long-standing argument that a network’s sensitivity to adversarial examples is tied to its spectral properties and hints at novel ways to robustify and defend against adversarial attacks. We provide extensive empirical evidence on state-of-the-art network architectures to support our theoretical results.

1. Introduction

Deep neural networks have been used with great success for perceptual tasks such as image classification (Simonyan & Zisserman, 2014; LeCun et al., 2015) or speech recognition (Hinton et al., 2012). While they are known to be robust to random noise, it has been shown that the accuracy of deep nets dramatically deteriorates in the face of so-called adversarial examples (Biggio et al., 2013; Szegedy et al., 2013; Goodfellow et al., 2014), i.e. small perturbations of the input signal, often imperceptible to humans, that are sufficient to induce large changes in the model output. This apparent vulnerability is worrisome as deep nets start to proliferate in the real-world, including in safety-critical deployments. Consequently, there has been a surge in methods that find adversarial perturbations (Sabour et al., 2015; Papernot et al., 2016; Kurakin et al., 2016; Moosavi-Dezfooli et al., 2016; Moosavi-Dezfooli et al., 2017; Madry et al., 2017; Athalye et al., 2018).

The most direct strategy of robustification, called adversar-

^{*}Equal contribution ¹Department of Computer Science, ETH Zürich. Correspondence to: <kevin.roth@inf.ethz.ch>, <yannic.kilcher@inf.ethz.ch>, <thomas.hofmann@inf.ethz.ch>.

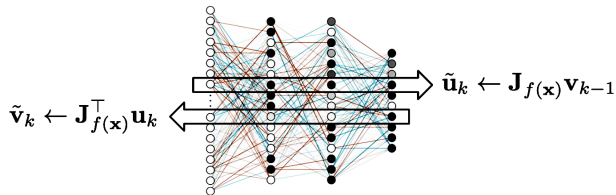


Figure 1. Our theoretical results suggest to think of iterative adversarial attacks as power-method-like forward-backward passes through (the Jacobian $\mathbf{J}_f(\mathbf{x})$ of) the network. The precise statement and notation can be found in Theorem 1 and Section 4.

ial training, aims to harden a machine learning model by training it against an adversary that maliciously corrupts examples before passing them to the model (Goodfellow et al., 2014; Kurakin et al., 2016; Miyato et al., 2015; 2017; Madry et al., 2017). A different strategy of defense is to detect whether the input has been perturbed via characteristic regularities either in the adversarial perturbations themselves or in the network activations they induce (Grosse et al., 2017; Feinman et al., 2017; Xu et al., 2017; Metzen et al., 2017; Carlini & Wagner, 2017; Roth et al., 2019).

Despite practical advances in finding adversarial examples and defending against them, it is still an open question whether (i) adversarial examples are unavoidable, i.e. no robust model exists, cf. (Fawzi et al., 2018; Gilmer et al., 2018), (ii) learning a robust model requires too much training data, cf. (Schmidt et al., 2018), (iii) learning a robust model from limited training data is possible but computationally intractable (Bubeck et al., 2018), or (iv) we just have not found the right model / training algorithm yet, i.e. adversarial examples can ultimately be overcome.

In this work, we investigate the origin of adversarial vulnerability in neural networks by focusing on the attack algorithms used to find adversarial examples. In particular, we make the following contributions:

- We present a data-dependent variant of spectral norm regularization that directly regularizes large singular values of a neural network in regions that are supported by the data, as opposed to existing methods that regularize a global, data-independent upper bound.

- We establish a theoretical link between adversarial training and operator norm regularization for deep neural networks. Specifically, we prove that ℓ_p -norm constrained projected gradient ascent with an ℓ_q -norm loss on the logits of clean and perturbed inputs is equivalent to data-dependent (p, q) operator norm regularization.
- We conduct extensive empirical evaluations showing that (i) adversarial perturbations align with dominant singular vectors, (ii) adversarial training dampens the singular values, and (iii) adversarial training and data-dependent spectral norm regularization give rise to models that are significantly more linear around data.

2. Related Work

The idea that a conservative measure of the sensitivity of a network against adversarial examples can be obtained by computing the spectral norm of the individual weight layers appeared already in the seminal work of Szegedy et al. (2013). A number of works have since suggested to regularize the spectral norm (Yoshida & Miyato, 2017; Miyato et al., 2018; Bartlett et al., 2017; Farnia et al., 2018) and Lipschitz constant (Cisse et al., 2017; Hein & Andriushchenko, 2017; Tsuzuku et al., 2018; Raghunathan et al., 2018) as a means to improve model robustness against adversarial attacks. In the same vein, training methods based on input gradient regularization have been proposed (Gu & Rigazio, 2014; Lyu et al., 2015; Cisse et al., 2017).

The most direct and popular strategy of robustification, however, is to use adversarial examples as data augmentation during training (Goodfellow et al., 2014; Shaham et al., 2015; Kurakin et al., 2016; Miyato et al., 2017; Madry et al., 2017). Adversarial training can be viewed as a variant of (distributionally) robust optimization (El Ghaoui & Le Bret, 1997; Xu et al., 2009; Bertsimas & Copenhaver, 2018; Namkoong & Duchi, 2017; Sinha et al., 2017; Gao & Kleywegt, 2016) where a machine learning model is trained to minimize the worst-case loss against an adversary that can shift the entire training data within an uncertainty set. Interestingly, for certain problems and uncertainty sets, such as for linear regression and induced matrix norm balls, robust optimization has been shown to be equivalent to regularization (El Ghaoui & Le Bret, 1997; Xu et al., 2009; Bertsimas & Copenhaver, 2018; Bietti et al., 2018). Similar results on the equivalence of robustness and regularization have been obtained also for (kernelized) SVMs (Xu et al., 2009).

More recently, related works have started to develop a learning theory for robust optimization, including Lipschitz-sensitive generalization bounds (Neyshabur et al., 2015) and spectrally-normalized margin bounds for neural networks (Bartlett et al., 2017), particularly as bounds on the (global) spectral norm or Lipschitz constant can easily be translated

to bounds on the minimal perturbation required to fool a machine learning model.

We extend these lines of work by establishing a theoretical link between adversarial training and data-dependent operator norm regularization. This fundamental connection confirms the long-standing argument that a network’s sensitivity to adversarial examples is tied to its spectral properties and opens the door for adversarially robust generalization bounds via data-dependent spectral norm based ones.

3. Background

3.1. Global Spectral Norm Regularization

In this section we rederive spectral norm regularization à la Yoshida & Miyato (2017), while also setting up the notation for later. Let \mathbf{x} and y denote input-label pairs generated from a data distribution P . Let $f : \mathcal{X} \subset \mathbb{R}^n \rightarrow \mathbb{R}^d$ denote the logits of a θ -parameterized piecewise linear classifier, i.e. $f(\cdot) = \mathbf{W}^L \phi^{L-1}(\mathbf{W}^{L-1} \phi^{L-2}(\dots) + \mathbf{b}^{L-1}) + \mathbf{b}^L$, where ϕ^ℓ is the activation function, and $\mathbf{W}^\ell, \mathbf{b}^\ell$ denote the layer-wise weight matrix¹ and bias vector, collectively denoted by θ . Let us furthermore assume that each activation function is a ReLU (the argument can easily be generalized to other piecewise linear activations). In this case, the activations ϕ^ℓ act as input-dependent diagonal matrices $\Phi_{\mathbf{x}}^\ell := \text{diag}(\phi_{\mathbf{x}}^\ell)$, where an element in the diagonal $\phi_{\mathbf{x}}^\ell := \mathbf{1}(\tilde{\mathbf{x}}^\ell \geq 0)$ is one if the corresponding pre-activation $\tilde{\mathbf{x}}^\ell := \mathbf{W}^\ell \phi^{\ell-1}(\cdot) + \mathbf{b}^\ell$ is positive and zero otherwise.

Following Raghu et al. (Raghu et al., 2017), we call $\phi_{\mathbf{x}} := (\phi_{\mathbf{x}}^1, \dots, \phi_{\mathbf{x}}^{L-1}) \in \{0, 1\}^m$ the “activation pattern”, where m is the number of neurons in the network. For any activation pattern $\phi \in \{0, 1\}^m$ we can define the preimage $X(\phi) := \{\mathbf{x} \in \mathbb{R}^n : \phi_{\mathbf{x}} = \phi\}$, inducing a partitioning of the input space via $\mathbb{R}^n = \bigcup_{\phi} X(\phi)$. Note that some $X(\phi) = \emptyset$, as not all combinations of activations may be feasible. See Figure 1 in (Raghu et al., 2017) or Figure 3 in (Novak et al., 2018) for an illustration of ReLU tessellations of the input space.

We can linearize f at \mathbf{x} with its Jacobian $\mathbf{J}_f(\mathbf{x})$

$$f(\mathbf{x} + \Delta\mathbf{x}) \simeq f(\mathbf{x}) + \mathbf{J}_f(\mathbf{x})\Delta\mathbf{x}, \tag{1}$$

with equality if $\mathbf{x} + \Delta\mathbf{x} \in X(\phi_{\mathbf{x}})$, and where

$$\mathbf{J}_f(\mathbf{x}) = \mathbf{W}^L \cdot \Phi_{\mathbf{x}}^{L-1} \cdot \mathbf{W}^{L-1} \cdot \Phi_{\mathbf{x}}^{L-2} \dots \Phi_{\mathbf{x}}^1 \cdot \mathbf{W}^1. \tag{2}$$

We have the following bound for small $\|\Delta\mathbf{x}\|_2 \neq 0$

$$\frac{\|f(\mathbf{x} + \Delta\mathbf{x}) - f(\mathbf{x})\|_2}{\|\Delta\mathbf{x}\|_2} \simeq \frac{\|\mathbf{J}_f(\mathbf{x})\Delta\mathbf{x}\|_2}{\|\Delta\mathbf{x}\|_2} \leq \sigma(\mathbf{J}_f(\mathbf{x})) \tag{3}$$

¹Note that convolutional layers can be constructed as matrix multiplications by converting the convolution operator into a Toeplitz matrix.

where $\sigma(\mathbf{J}_f(\mathbf{x}))$ is the *spectral norm* (largest singular value) of the linear operator $\mathbf{J}_f(\mathbf{x})$,

$$\sigma(\mathbf{J}_f(\mathbf{x})) := \max_{\mathbf{v}: \|\mathbf{v}\|_2=1} \|\mathbf{J}_f(\mathbf{x})\mathbf{v}\|_2 \quad (4)$$

From a robustness perspective we want $\sigma(\mathbf{J}_f(\mathbf{x}))$ to be small in regions that are supported by the data.

Based on the factorization in Equation 2 and the non-expansiveness of the activations, $\sigma(\Phi_{\mathbf{x}}^\ell) \leq 1$ for every $\ell \in \{1, \dots, L-1\}$, Yoshida & Miyato (2017) suggest to upper-bound the spectral norm of the Jacobian by the product of the spectral norms of the individual weight matrices

$$\sigma(\mathbf{J}_f(\mathbf{x})) \leq \prod_{\ell=1}^L \sigma(\mathbf{W}^\ell) \quad , \quad \forall \mathbf{x} \in \mathcal{X} . \quad (5)$$

The layer-wise spectral norms $\sigma^\ell := \sigma(\mathbf{W}^\ell)$ can be computed iteratively using the power method². Starting with a random vector \mathbf{v}_0 , the power method iteratively computes

$$\begin{aligned} \mathbf{u}_k^\ell &\leftarrow \tilde{\mathbf{u}}_k^\ell / \|\tilde{\mathbf{u}}_k^\ell\|_2, \quad \tilde{\mathbf{u}}_k^\ell \leftarrow \mathbf{W}^\ell \mathbf{v}_{k-1}^\ell \\ \mathbf{v}_k^\ell &\leftarrow \tilde{\mathbf{v}}_k^\ell / \|\tilde{\mathbf{v}}_k^\ell\|_2, \quad \tilde{\mathbf{v}}_k^\ell \leftarrow (\mathbf{W}^\ell)^\top \mathbf{u}_k^\ell . \end{aligned} \quad (6)$$

The (final) singular value is $\sigma_k^\ell = (\mathbf{u}_k^\ell)^\top \mathbf{W}^\ell \mathbf{v}_k^\ell$.

Yoshida & Miyato (2017) suggest to turn this upper-bound into a global (data-independent) regularizer by learning the parameters θ via penalized empirical risk minimization

$$\min \theta \rightarrow \mathbf{E}_{(\mathbf{x}, y) \sim \hat{P}} [\ell(y, f(\mathbf{x}))] + \frac{\lambda}{2} \sum_{\ell=1}^L \sigma(\mathbf{W}^\ell)^2, \quad (7)$$

where $\ell(\cdot, \cdot)$ denotes an arbitrary classification loss. It can be verified that $\nabla_{\mathbf{W}} \sigma(\mathbf{W})^2 / 2 = \sigma \mathbf{u} \mathbf{v}^\top$, with σ , \mathbf{u} and \mathbf{v} being the principal singular value/vectors of \mathbf{W} , Equation 7 effectively adds a term $\lambda \sigma^\ell \mathbf{u}^\ell (\mathbf{v}^\ell)^\top$ to the parameter gradient of each layer ℓ . In terms of computational complexity, because the global regularizer decouples from the empirical loss, the power-method can be amortized across data-points, hence a single power method iteration per parameter update step usually suffices in practice (Yoshida & Miyato, 2017).

3.2. Global vs. Local Regularization

The advantage of global bounds is that they trivially generalize from the training to the test set. The problem however is that they can be arbitrarily loose, e.g. penalizing the spectral norm over irrelevant regions of the ambient space. To illustrate this, consider the ideal robust classifier that is essentially piecewise constant on class-conditional regions, with sharp transitions between the classes. The global spectral norm will be heavily influenced by the sharp transition zones, whereas a local data-dependent bound can adapt to regions where the classifier is approximately constant (Hein & Andriushchenko, 2017). We would therefore expect a global regularizer to have the largest effect in the empty parts of the input space. A local regularizer, on the contrary, has its main effect around the data manifold.

4. Adversarial Training is a Form of Operator Norm Regularization

4.1. Data-dependent Spectral Norm Regularization

We now show how to directly regularize the *data-dependent* spectral norm of the Jacobian $\mathbf{J}_f(\mathbf{x})$. Under the assumption that the dominant singular value is non-degenerate², the problem of computing the largest singular value and the corresponding left and right singular vectors can efficiently be solved via the power method. Starting from \mathbf{v}_0 ,

$$\begin{aligned} \mathbf{u}_k &\leftarrow \tilde{\mathbf{u}}_k / \|\tilde{\mathbf{u}}_k\|_2, \quad \tilde{\mathbf{u}}_k \leftarrow \mathbf{J}_f(\mathbf{x}) \mathbf{v}_{k-1} \\ \mathbf{v}_k &\leftarrow \tilde{\mathbf{v}}_k / \|\tilde{\mathbf{v}}_k\|_2, \quad \tilde{\mathbf{v}}_k \leftarrow \mathbf{J}_f(\mathbf{x})^\top \mathbf{u}_k \end{aligned} \quad (8)$$

The (final) singular value can then be computed via $\sigma(\mathbf{J}_f(\mathbf{x})) = \mathbf{u}^\top \mathbf{J}_f(\mathbf{x}) \mathbf{v}$, where \mathbf{u} and \mathbf{v} are computed via Equation 8. For brevity we suppress the dependence of \mathbf{u} , \mathbf{v} on \mathbf{x} in the rest of the paper. Note that the right singular vector \mathbf{v} gives the direction in input space that corresponds to the steepest ascent of $f(\mathbf{x})$ along \mathbf{u} . See Figure 1 for an illustration of the forward-backward passes through (the Jacobian $\mathbf{J}_f(\mathbf{x})$ of) the network.

We can turn this into a regularizer by learning the parameters θ via the following Jacobian-based spectral norm penalized empirical risk minimization

$$\min \theta \rightarrow \mathbf{E}_{(\mathbf{x}, y) \sim \hat{P}} \left[\ell(y, f(\mathbf{x})) + \frac{\tilde{\lambda}}{2} \sigma(\mathbf{J}_f(\mathbf{x}))^2 \right], \quad (9)$$

where the data-dependent singular value $\sigma(\mathbf{J}_f(\mathbf{x}))$ is computed via Equation 8.

By optimality / stationarity³ we also have that $\sigma(\mathbf{J}_f(\mathbf{x})) = \mathbf{u}^\top \mathbf{J}_f(\mathbf{x}) \mathbf{v} = \|\mathbf{J}_f(\mathbf{x}) \mathbf{v}\|_2$. Together with linearization $\epsilon \mathbf{J}_f(\mathbf{x}) \mathbf{v} \simeq f(\mathbf{x} + \epsilon \mathbf{v}) - f(\mathbf{x})$ (which holds with equality if $\mathbf{x} + \epsilon \mathbf{v} \in X(\phi_{\mathbf{x}})$), we can regularize learning also via a sum-of-squares based spectral norm regularizer $\frac{\lambda}{2} \|f(\mathbf{x} + \epsilon \mathbf{v}) - f(\mathbf{x})\|_2^2$, where the data-dependent singular vector \mathbf{v} of $\mathbf{J}_f(\mathbf{x})$ is computed via Equation 8 and $\tilde{\lambda} = \lambda \epsilon^2$. Both variants can readily be implemented in modern deep learning frameworks. We found the sum-of-squares based one to be slightly more numerically stable.

In terms of computational complexity, the data-dependent regularizer is equally expensive as PGA-based adversarial training, and both are a constant (number of power method iterations) times more expensive than the data-independent variant, plus an overhead that depends on the batch size, which is usually mitigated in modern frameworks by parallelizing computations across a batch of data.

²Due to numerical errors, we can safely assume that the dominant singular value is non-degenerate.

³ $\mathbf{u} = \mathbf{J}_f(\mathbf{x}) \mathbf{v} / \|\mathbf{J}_f(\mathbf{x}) \mathbf{v}\|_2$. Compare with the definition of the spectral norm in Equation 4 and the (2,2)-operator norm (= spectral norm) in Equation 10.

4.2. Data-dependent Operator Norm Regularization

More generally, we can directly regularize the data-dependent (p, q) -operator norm of the Jacobian $\mathbf{J}_f(\mathbf{x})$. To this end, let the input-space (domain) and output-space (co-domain) of the linear map $\mathbf{J}_f(\mathbf{x})$ be equipped with the ℓ_p and ℓ_q norms respectively, defined as $\|\mathbf{x}\|_p := (\sum_{i=1}^n |x_i|^p)^{1/p}$ for $1 \leq p < \infty$ and $\|\mathbf{x}\|_\infty := \max_i |x_i|$ for $p = \infty$. The *data-dependent (p, q) -operator norm of $\mathbf{J}_f(\mathbf{x})$* is defined as

$$\|\mathbf{J}_f(\mathbf{x})\|_{p,q} := \max_{\mathbf{v}: \|\mathbf{v}\|_p=1} \|\mathbf{J}_f(\mathbf{x})\mathbf{v}\|_q \quad (10)$$

which is a (data-dependent) measure of the maximal amount of signal-gain that can be induced when propagating a norm-bounded input vector through the linearized network. Table 1 shows (p, q) -operator norms for typical values of p (domain) and q (co-domain).

For general (p, q) -norms, the maximizer \mathbf{v} in Equation 10 can be computed via projected gradient ascent. Let \mathbf{v}_0 be a random vector or an approximation to the maximizer. The data-dependent (p, q) -operator norm of $\mathbf{J}_f(\mathbf{x})$ can be computed iteratively via

$$\mathbf{v}_k = \Pi_{\{\|\cdot\|_p=1\}}(\mathbf{v}_{k-1} + \alpha \nabla_{\mathbf{v}} \|\mathbf{J}_f(\mathbf{x})\mathbf{v}_{k-1}\|_q) \quad (11)$$

where $\Pi_{\{\|\cdot\|_p=1\}}(\tilde{\mathbf{v}}) := \arg \min_{\mathbf{v}^*: \|\mathbf{v}^*\|_p=1} \|\mathbf{v}^* - \tilde{\mathbf{v}}\|_2$ is the orthogonal projection (normalization) onto the ℓ_p unit sphere, and where α is a step-size or weighting factor, trading off the previous iterate \mathbf{v}_{k-1} with the current gradient step $\nabla_{\mathbf{v}} \|\mathbf{J}_f(\mathbf{x})\mathbf{v}_{k-1}\|_q$.

By the chain-rule, the computation of the gradient step

$$\nabla_{\mathbf{v}} \|\mathbf{J}_f(\mathbf{x})\mathbf{v}\|_q = \mathbf{J}_f(\mathbf{x})^\top \text{sign}(\mathbf{u}) \odot |\mathbf{u}|^{q-1} / \|\mathbf{u}\|_q^{q-1} \quad (12)$$

where $\mathbf{u} = \mathbf{J}_f(\mathbf{x})\mathbf{v}$, can be decomposed into a forward and backward pass through the Jacobian $\mathbf{J}_f(\mathbf{x})$, yielding the following *projected gradient ascent based operator norm iteration method*

$$\begin{aligned} \mathbf{u}_k &\leftarrow \text{sign}(\tilde{\mathbf{u}}_k) \odot |\tilde{\mathbf{u}}_k|^{q-1} / \|\tilde{\mathbf{u}}_k\|_q^{q-1}, \quad \tilde{\mathbf{u}}_k \leftarrow \mathbf{J}_f(\mathbf{x})\mathbf{v}_{k-1} \\ \mathbf{v}_k &\leftarrow \Pi_{\{\|\cdot\|_p=1\}}(\mathbf{v}_{k-1} + \alpha \tilde{\mathbf{v}}_k), \quad \tilde{\mathbf{v}}_k \leftarrow \mathbf{J}_f(\mathbf{x})^\top \mathbf{u}_k \end{aligned} \quad (13)$$

where \odot , $\text{sign}(\cdot)$ and $|\cdot|$ denote elementwise product, sign and absolute-value. See Figure 1 for an illustration of the forward-backward passes through the Jacobian $\mathbf{J}_f(\mathbf{x})$.

In particular, we have the following well-known special cases. For $q = 2$, the forward pass equation is given by $\mathbf{u}_k \leftarrow \tilde{\mathbf{u}}_k / \|\tilde{\mathbf{u}}_k\|_2$, while for $q = 1$ it is given by $\mathbf{u}_k \leftarrow \text{sign}(\tilde{\mathbf{u}}_k)$. The $q = \infty$ limit on the other hand is given by

$$\lim_{q \rightarrow \infty} \text{sign}(\tilde{\mathbf{u}}) \odot |\tilde{\mathbf{u}}|^{q-1} / \|\tilde{\mathbf{u}}\|_q^{q-1} = \frac{1}{|\mathcal{I}|} \text{sign}(\tilde{\mathbf{u}}) \odot \mathbf{1}_{\mathcal{I}} \quad (14)$$

with $\mathbf{1}_{\mathcal{I}} = \sum_{i \in \mathcal{I}} \mathbf{e}_i$, where $\mathcal{I} := \{j \in [1, \dots, d] : |\tilde{u}_j| = \|\tilde{\mathbf{u}}\|_\infty\}$ denotes the set of indices at which $\tilde{\mathbf{u}}$ attains its

Table 1. Computing (p, q) -operator norms for typical values of p (domain) and q (co-domain). See Section 4.3.1 in (Tropp, 2004). We prove equivalence between data-dependent (p, q) -operator norm regularization and adversarial training based on ℓ_p -norm constrained projected gradient ascent with an ℓ_q -norm loss on the logits of the clean and perturbed inputs for all the norms in this table. In our setting, ‘‘columns’’ of $\mathbf{J}_f(\mathbf{x})$ correspond to paths through the network originating in a specific input neuron, whereas ‘‘rows’’ correspond to paths ending in a specific output neuron.

		Co-domain		
		ℓ_1	ℓ_2	ℓ_∞
Domain	ℓ_1	max ℓ_1 norm of a column	max ℓ_2 norm of a column	max ℓ_∞ norm of a column
	ℓ_2	NP-hard	max singular value	max ℓ_2 norm of a row
	ℓ_∞	NP-hard	NP-hard	max ℓ_1 norm of a row

maximum norm and \mathbf{e}_i is the i -th canonical unit vector. See Section 7.5 in the Appendix for a derivation.

It is interesting to note that we can recover the power method update equations by taking the limit $\alpha \rightarrow \infty$ in the above projected gradient ascent based operator norm iteration equations, which we consider to be an interesting result in its own right. In fact, we have the following useful Lemma 2 (Projection Lemma)

$$\lim_{\alpha \rightarrow \infty} \Pi_{\{\|\cdot\|_p=1\}}(\mathbf{v} + \alpha \tilde{\mathbf{v}}) = \frac{\text{sign}(\tilde{\mathbf{v}}) \odot |\tilde{\mathbf{v}}|^{p^*-1}}{\|\tilde{\mathbf{v}}\|_{p^*}^{p^*-1}} \quad (15)$$

where p^* is the Hölder conjugate given by $1/p + 1/p^* = 1$. Note that the limit is well-defined since α is inside the projection operation. The proof can be found in Section 7.3 in the Appendix. With this, we obtain the following *power method limit* of the operator norm iteration equations

$$\begin{aligned} \mathbf{u}_k &\leftarrow \text{sign}(\tilde{\mathbf{u}}_k) \odot |\tilde{\mathbf{u}}_k|^{q-1} / \|\tilde{\mathbf{u}}_k\|_q^{q-1}, \quad \tilde{\mathbf{u}}_k \leftarrow \mathbf{J}_f(\mathbf{x})\mathbf{v}_{k-1} \\ \mathbf{v}_k &\leftarrow \text{sign}(\tilde{\mathbf{v}}_k) \odot |\tilde{\mathbf{v}}_k|^{p^*-1} / \|\tilde{\mathbf{v}}_k\|_{p^*}^{p^*-1}, \quad \tilde{\mathbf{v}}_k \leftarrow \mathbf{J}_f(\mathbf{x})^\top \mathbf{u}_k \end{aligned} \quad (16)$$

Compare this with the Power Method Algorithm in Section 2 of (Higham, 1992). See (Boyd, 1974; Higham, 1992) for a convergence analysis of the power method. The condition that $\alpha \rightarrow \infty$ means that in the update equation for \mathbf{v}_k all the weight is placed on the current gradient direction $\tilde{\mathbf{v}}_k$ whereas no weight is put on the previous iterate \mathbf{v}_{k-1} .

We can turn this into a regularizer by learning the parameters θ via the following operator-norm regularized objective

$$\min_{\theta} \theta \rightarrow \mathbf{E}_{(\mathbf{x}, y) \sim \hat{P}} \left[\ell(y, f(\mathbf{x})) + \tilde{\lambda} \|\mathbf{J}_f(\mathbf{x})\|_{p,q} \right] \quad (17)$$

Note that we can also use the q -th power of the operator norm as a regularizer (with a prefactor of $1/q$). It is easy to see that this only affects the normalization of \mathbf{u}_k , since $\nabla_{\mathbf{v}} \frac{1}{q} \|\mathbf{J}_f(\mathbf{x})\mathbf{v}\|_q^q = \|\mathbf{J}_f(\mathbf{x})\mathbf{v}\|_q^{q-1} \nabla_{\mathbf{v}} \|\mathbf{J}_f(\mathbf{x})\mathbf{v}\|_q$.

4.3. PowerMethod Formulation of Adversarial Training

Adversarial training (Goodfellow et al., 2014; Kurakin et al., 2016; Madry et al., 2017) aims to improve the robustness of a machine learning model by training it against an adversary that independently perturbs each training example subject to a proximity constraint, e.g. in ℓ_p -norm,

$$\min \theta \rightarrow \mathbf{E}_{(\mathbf{x}, y) \sim \hat{P}} \left[\ell(y, f(\mathbf{x})) + \lambda \max_{\mathbf{x}^* \in \mathcal{B}_\epsilon^p(\mathbf{x})} \ell_{\text{adv}}(y, f(\mathbf{x}^*)) \right] \quad (18)$$

where $\ell_{\text{adv}}(\cdot, \cdot)$ denotes the loss function used to find adversarial perturbations (which is not necessarily the same as the classification loss $\ell(\cdot, \cdot)$).

The adversarial example \mathbf{x}^* is typically computed iteratively, e.g. via ℓ_p -norm constrained projected gradient ascent (cf. for instance the Projected Gradient Descent attack in the cleverhans library (Papernot et al., 2017) or Section 3 on PGD-based adversarial attacks in (Wong et al., 2019))⁴:

$$\begin{aligned} \mathbf{x}_0 &\sim \mathcal{U}(\mathcal{B}_\epsilon^p(\mathbf{x})) \\ \mathbf{x}_k &= \Pi_{\mathcal{B}_\epsilon^p(\mathbf{x})} \left(\mathbf{x}_{k-1} + \alpha \arg \max_{\mathbf{v}_k: \|\mathbf{v}_k\|_p \leq 1} \mathbf{v}_k^\top \nabla_{\mathbf{x}} \ell_{\text{adv}}(y, f(\mathbf{x}_{k-1})) \right) \end{aligned} \quad (19)$$

where $\Pi_{\mathcal{B}_\epsilon^p(\mathbf{x})}(\tilde{\mathbf{x}}) := \arg \min_{\mathbf{x}^* \in \mathcal{B}_\epsilon^p(\mathbf{x})} \|\mathbf{x}^* - \tilde{\mathbf{x}}\|_2$ is the orthogonal projection operator into the norm ball $\mathcal{B}_\epsilon^p(\mathbf{x}) := \{\mathbf{x}^* : \|\mathbf{x}^* - \mathbf{x}\|_p \leq \epsilon\}$, α is a step-size or weighting factor, trading off the previous iterate \mathbf{x}_{k-1} with the current gradient step \mathbf{v}_k , and y is the true or predicted label. For targeted attacks the sign in front of α is flipped, so as to descend the loss function into the direction of the target label.

In fact, we can derive the following explicit expression for the optimal perturbation to a linear function under an ℓ_p -norm constraint⁵, Lemma 1 (Optimal Perturbation),

$$\mathbf{v}^* = \arg \max_{\mathbf{v}: \|\mathbf{v}\|_p \leq 1} \mathbf{v}^\top \mathbf{z} = \frac{\text{sign}(\mathbf{z}) \odot |\mathbf{z}|^{p^*-1}}{\|\mathbf{z}\|_{p^*}^{p^*-1}} \quad (20)$$

where \odot , $\text{sign}(\cdot)$ and $|\cdot|$ denote elementwise product, sign and absolute-value, p^* is the Hölder conjugate of p , given by $1/p + 1/p^* = 1$, and \mathbf{z} is an arbitrary non-zero vector, e.g. $\mathbf{z} = \nabla_{\mathbf{x}} \ell_{\text{adv}}(y, f(\mathbf{x}))$. We note that the above expression for the maximizer has already been stated in the DeepFool paper (Moosavi Dezfooli et al., 2016). The derivation can be found in Section 7.2 in the Appendix.

As a result, ℓ_p -norm constrained projected gradient ascent

⁴In principle we could take a different norm in the inner maximization than for the projection. Our results can easily be extended to this slightly more general case (just replace p^* with q^*).

⁵Note that for $p \in \{1, \infty\}$ the maximizer might not be unique, in which case we simply choose a specific representative. See Section 7.2 for more details.

can therefore be implemented as follows

$$\mathbf{x}_k = \Pi_{\mathcal{B}_\epsilon^p(\mathbf{x})} \left(\mathbf{x}_{k-1} + \alpha \frac{\text{sign}(\nabla_{\mathbf{x}} \ell_{\text{adv}}) \odot |\nabla_{\mathbf{x}} \ell_{\text{adv}}|^{p^*-1}}{\|\nabla_{\mathbf{x}} \ell_{\text{adv}}\|_{p^*}^{p^*-1}} \right) \quad (21)$$

where p^* is given by $1/p + 1/p^* = 1$ and $\nabla_{\mathbf{x}} \ell_{\text{adv}}$ is shorthand notation for $\nabla_{\mathbf{x}} \ell_{\text{adv}}(y, f(\mathbf{x}_{k-1}))$.

The most common variants are ℓ_2 -norm and ℓ_∞ -norm constrained PGA (Madry et al., 2017; Kurakin et al., 2016)

$$\begin{aligned} \mathbf{x}_k &= \Pi_{\mathcal{B}_\epsilon^2(\mathbf{x})} \left(\mathbf{x}_{k-1} + \alpha \frac{\nabla_{\mathbf{x}} \ell_{\text{adv}}(y, f(\mathbf{x}_{k-1}))}{\|\nabla_{\mathbf{x}} \ell_{\text{adv}}(y, f(\mathbf{x}_{k-1}))\|_2} \right), \quad [\ell_2] \\ \mathbf{x}_k &= \Pi_{\mathcal{B}_\epsilon^\infty(\mathbf{x})} \left(\mathbf{x}_{k-1} + \alpha \text{sign}(\nabla_{\mathbf{x}} \ell_{\text{adv}}(y, f(\mathbf{x}_{k-1}))) \right), \quad [\ell_\infty] \end{aligned} \quad (22)$$

By the chain-rule, the computation of the gradient-step $\tilde{\mathbf{v}}_k := \nabla_{\mathbf{x}} \ell_{\text{adv}}(y, f(\mathbf{x}_{k-1}))$ can be decomposed into a logit-gradient and a Jacobian vector product. The ℓ_p -norm constrained projected gradient ascent attack can thus equivalently be written in the following power method like forward-backward pass form (the normalization of $\tilde{\mathbf{u}}_k$ is optional and can be absorbed into the normalization of $\tilde{\mathbf{v}}_k$)

$$\begin{aligned} \mathbf{u}_k &\leftarrow \tilde{\mathbf{u}}_k / \|\tilde{\mathbf{u}}_k\|_2, \quad \tilde{\mathbf{u}}_k \leftarrow \nabla_{\mathbf{z}} \ell_{\text{adv}}(y, \mathbf{z})|_{\mathbf{z}=f(\mathbf{x}_{k-1})} \\ \mathbf{v}_k &\leftarrow \frac{\text{sign}(\tilde{\mathbf{v}}_k) \odot |\tilde{\mathbf{v}}_k|^{p^*-1}}{\|\tilde{\mathbf{v}}_k\|_{p^*}^{p^*-1}}, \quad \tilde{\mathbf{v}}_k \leftarrow \mathbf{J}_f(\mathbf{x}_{k-1})^\top \mathbf{u}_k \\ \mathbf{x}_k &\leftarrow \Pi_{\mathcal{B}_\epsilon^p(\mathbf{x})}(\mathbf{x}_{k-1} + \alpha \mathbf{v}_k) \end{aligned} \quad (23)$$

Note that the logit-gradient $\nabla_{\mathbf{z}} \ell_{\text{adv}}(y, \mathbf{z})|_{\mathbf{z}=f(\mathbf{x}_{k-1})}$ can be computed in a single forward pass, by directly expressing it in terms of the arguments of the adversarial loss.

In particular, for an ℓ_q -norm loss on the logits of the clean and perturbed input $\ell_{\text{adv}}(f(\mathbf{x}), f(\mathbf{x}^*)) = \|f(\mathbf{x}) - f(\mathbf{x}^*)\|_q$, the forward-backward pass equations become

$$\begin{aligned} \mathbf{u}_k &\leftarrow \frac{\text{sign}(\tilde{\mathbf{u}}_k) \odot |\tilde{\mathbf{u}}_k|^{q-1}}{\|\tilde{\mathbf{u}}_k\|_q^{q-1}}, \quad \tilde{\mathbf{u}}_k \leftarrow f(\mathbf{x}_{k-1}) - f(\mathbf{x}) \\ \mathbf{v}_k &\leftarrow \frac{\text{sign}(\tilde{\mathbf{v}}_k) \odot |\tilde{\mathbf{v}}_k|^{p^*-1}}{\|\tilde{\mathbf{v}}_k\|_{p^*}^{p^*-1}}, \quad \tilde{\mathbf{v}}_k \leftarrow \mathbf{J}_f(\mathbf{x}_{k-1})^\top \mathbf{u}_k \end{aligned} \quad (24)$$

See Section 7.6 in the Appendix for an example using the softmax cross-entropy loss.

Comparing the update equations for projected gradient ascent based adversarial training with those of data-dependent operator norm regularization, we can see that *adversarial training is a form of the data-dependent operator norm regularization*. The three degrees of freedom of adversarial training are: (i) the choice of the adversarial loss function, (ii) the choice of ϵ -ball to project into, and (iii) the step-size or weighting factor α .

The following theorem states the precise conditions under which projected gradient ascent based adversarial training is equivalent to data-dependent operator norm regularization. The proof can be found in Section 7.4 in the Appendix.

Theorem 1. For ϵ small enough such that $\mathcal{B}_\epsilon^p(\mathbf{x}) \subset X(\phi_{\mathbf{x}})$ and in the limit $\alpha \rightarrow \infty$, ℓ_p -norm constrained projected gradient ascent based adversarial training with an ℓ_q -norm loss on the logits of the clean and perturbed input $\ell_{\text{adv}}(f(\mathbf{x}), f(\mathbf{x}^*)) = \|f(\mathbf{x}) - f(\mathbf{x}^*)\|_q$, with $p, q \in \{1, 2, \infty\}$, is equivalent to the power method limit of data-dependent (p, q) -operator norm regularization of the Jacobian $\mathbf{J}_f(\mathbf{x})$ of the network.

The conditions on ϵ and α can be considered specifics of the respective iteration method. The condition that ϵ be small enough such that $\mathcal{B}_\epsilon^p(\mathbf{x})$ is contained in the ReLU cell around \mathbf{x} ensures that $\mathbf{J}_f(\mathbf{x}^*) = \mathbf{J}_f(\mathbf{x})$ for all $\mathbf{x}^* \in \mathcal{B}_\epsilon^p(\mathbf{x})$. The power-method limit $\alpha \rightarrow \infty$ means that in the update equations all the weight is placed on the current gradient direction whereas no weight is put on the previous iterates.

Note that, in practice, the Theorem is applicable as long as the Jacobian of the network remains approximately constant in the uncertainty ball under consideration, in which case the correspondence between adversarial training and data-dependent operator norm regularization holds *approximately* in a region much larger than $X(\phi_{\mathbf{x}})$.

5. Experimental Results

5.1. Dataset, Architecture & Training Methods

We trained Convolutional Neural Networks (CNNs) with ReLU activations and batch normalization on the CIFAR10 data set (Krizhevsky & Hinton, 2009). We use a 7-layer CNN as our default platform, since it has good test set accuracy at acceptable computational requirements (we used an estimated 5k TitanX GPU hours in total for all our experiments). We train each classifier with a number of different training methods: (i) ‘Standard’: standard empirical risk minimization with a softmax cross-entropy loss, (ii) ‘Adversarial’: ℓ_2 -norm constrained projected gradient ascent (PGA) based adversarial training with a softmax cross-entropy loss, (iii) ‘global SNR’: global spectral norm regularization à la Yoshida & Miyato (Yoshida & Miyato, 2017), and (iv) ‘d.-d. SNR’: data-dependent spectral norm regularization. For the robustness experiments, we also train a state-of-the-art Wide Residual Network (WRN-28-10) (Zagoruyko & Komodakis, 2016).

As a default attack strategy we use an ℓ_2 -norm constrained PGA white-box attack with cross-entropy adversarial loss ℓ_{adv} and 10 attack iterations. We verified that all our conclusions also hold for larger numbers of attack iterations, however, due to computational constraints we limit the at-

Table 2. CIFAR10 test set accuracies on clean samples for the models and training methods we considered. The regularization constants were chosen such that the models achieve roughly the same accuracy on clean test examples as the adversarially trained model does. See Table 3 in Section 7.9 for the full setup. Results for global SNR with 10 iterations can be found in Section 7.13.

TRAINING METHOD	ACC. CNN7	ACC. WRN-28-10
STANDARD TRAINING	93.5%	96.3%
ADVERSARIAL TRAINING (10 ITERS)	83.6%	91.8%
DATA-DEP. SPECTRAL NORM (10 ITERS)	84.6%	91.3%
GLOBAL SPECTRAL NORM (1 ITERS)	80.4%	—

tack iterations to 10. The attack strength ϵ used for training was chosen to be the smallest value such that almost all adversarially perturbed inputs to the standard model are successfully misclassified, which is $\epsilon = 1.75$ (indicated by a vertical dashed line in the Figures below). The regularization constants of the other training methods were then chosen in such a way that they roughly achieve the same test set accuracy on clean examples as the adversarially trained model does. Further details regarding the experimental setup can be found in Section 7.8 in the Appendix. Table 2 summarizes the test set accuracies for the training methods we considered. Shaded areas in the plots below denote standard errors with respect to the number of test set samples over which the experiment was repeated.

Additional results against ℓ_∞ -norm constrained PGA attacks are provided in Section 7.14 in the Appendix. The conclusions remain the same for all the experiments we conducted.

5.2. Spectral Properties

Effect of training method on singular value spectrum.

We compute the singular value spectrum of the Jacobian $\mathbf{J}_{\phi^{L-1}}(\mathbf{x})$ for networks $f = \mathbf{W}\phi^{L-1}$ trained with different training methods and evaluated at a number of different test set examples (200 except if stated otherwise). Since we are interested in computing the full singular value spectrum, and not just the dominant singular value / vectors as during training, the power method would be too impractical, as it gives us access to only one (the dominant) singular value-vector pair at a time. Instead, we first extract the Jacobian (which is *per se* defined as a computational graph in modern deep learning frameworks) as an input-dim \times output-dim matrix and then use available matrix factorization routines to compute the full SVD of the extracted matrix. For each training method, the procedure is repeated for 200 randomly chosen clean and corresponding adversarially perturbed test set examples. Further details regarding the Jacobian extraction can be found in Section 7.7 in the Appendix.

The results are shown in Figure 2 (left). We can see that, compared to the spectrum of the normally trained and global

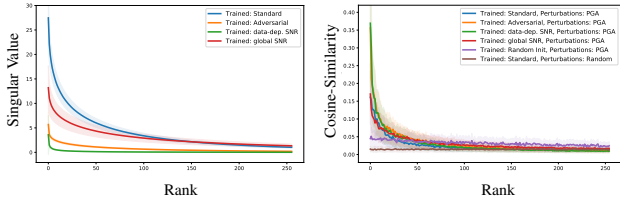


Figure 2. (Left) Singular value spectrum of the Jacobian $\mathbf{J}_{\phi^{L-1}}(\mathbf{x})$ for networks $f = \mathbf{W}^L \phi^{L-1}$ trained with different training methods. (Right) Cosine-similarity of adversarial perturbations with singular vectors \mathbf{v}_r of the Jacobian $\mathbf{J}_{\phi^{L-1}}(\mathbf{x})$, as a function of the rank r of the singular vector. For comparison we also show the cosine-similarity with the singular vectors of a random network as well as with random perturbations. Curves were aggregated over 200 samples from the test set. We can see that (i) adversarial training and data-dependent spectral norm regularization significantly dampen the singular values, and (ii) adversarial perturbations align with dominant singular vectors.

spectral norm regularized model, the spectrum of adversarially trained and data-dependent spectral norm regularized models is significantly damped after training. In fact, the data-dependent spectral norm regularizer seems to dampen the singular values even slightly more effectively than adversarial training, while global spectral norm regularization has almost no effect compared to standard training.

Alignment of adversarial perturbations with singular vectors. We compute the cosine-similarity of adversarial perturbations with singular vectors \mathbf{v}_r of the Jacobian $\mathbf{J}_{\phi^{L-1}}(\mathbf{x})$, extracted at a number of test set examples, as a function of the rank of the singular vectors returned by the SVD decomposition. For comparison we also show the cosine-similarity with the singular vectors of a random network as well with random perturbations.

The results are shown in Figure 2 (right). We can see that for all training methods (except the random network) adversarial perturbations are strongly aligned with the dominant singular vectors while the alignment decreases towards the bottom-ranked singular vectors. For the random network, the alignment is roughly constant with respect to rank. Interestingly, this strong alignment with dominant singular vectors also explains why input gradient regularization and fast gradient method (FGM) based adversarial training do not sufficiently protect against adversarial attacks, namely because the input gradient, resp. a single power method iteration, do not yield a sufficiently good approximation for the dominant singular vector in general.

5.3. Adversarial Robustness

Adversarial classification accuracy. A plot of the classification accuracy on adversarially perturbed test examples, as a function of the perturbation strength ϵ , is shown

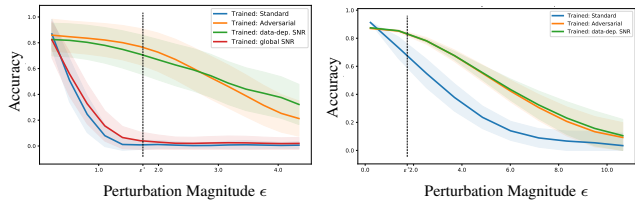


Figure 3. Classification accuracy as a function of perturbation strength ϵ . (Left) 7-layer CNN (Right) WideResNet WRN-28-10. The dashed line indicates the ϵ used during training. Curves were aggregated over 2000 (left) resp. all (right) samples from the test set. We can see that data-dependent spectral norm regularized models are equally robust to adversarial examples as adversarially trained models and both are significantly more robust than a normally trained one.

in Figure 3 (left) for the 7-layer CNN and (right) for the WideResNet WRN-28-10. We can see that data-dependent spectral norm regularized models are equally robust to adversarial examples as adversarially trained models and both are significantly more robust than a normally trained one, while global spectral norm regularization does not seem to robustify the model against adversarial attacks. This is in line with our earlier observation that adversarial perturbations tend to align with dominant singular vectors and that adversarial training and data-dependent spectral norm regularization dampen the singular values.

We also investigated the effect of varying α . Figure 6 in the Appendix shows the result of increasing the weighting factor α during adversarial training to very large values. As can be seen, the adversarial robustness initially rises, but after some threshold it levels out and does not change significantly even at very large values.

5.4. Local Linearity

Validity of linear approximation. In order to determine the size of the area where a locally linear approximation is valid, we measure the deviation from linearity of $\phi^{L-1}(\mathbf{x} + \mathbf{z})$ as the distance $\|\mathbf{z}\|_2$ to \mathbf{x} is increased in random and adversarial directions, i.e. we measure $\|\phi^{L-1}(\mathbf{x} + \mathbf{z}) - (\phi^{L-1}(\mathbf{x}) + \mathbf{J}_{\phi^{L-1}}(\mathbf{x})\mathbf{z})\|_2$ as a function of the distance $\|\mathbf{z}\|_2$, for random and adversarial perturbations \mathbf{z} , aggregated over 200 data points \mathbf{x} in the test set, with adversarial perturbations serving as a proxy for the direction in which the linear approximation holds the least. The purpose of this experiment is to investigate how good the linear approximation for different training methods is, as an increasing number of activation boundaries are crossed with increasing perturbation radius.

The results are shown in Figure 4 (left). We can see that adversarial training and data-dependent spectral norm regularization give rise to models that are considerably more

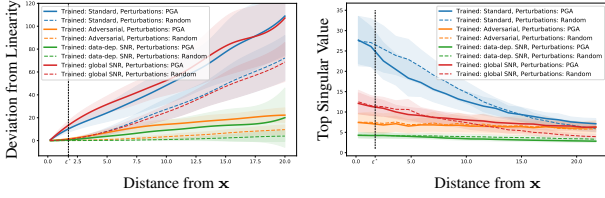


Figure 4. (Left) Deviation from linearity $\|\phi^{L-1}(\mathbf{x} + \mathbf{z}) - (\phi^{L-1}(\mathbf{x}) + \mathbf{J}_{\phi^{L-1}}(\mathbf{x})\mathbf{z})\|_2$ as a function of the distance $\|\mathbf{z}\|_2$ from \mathbf{x} for random and adversarial perturbations \mathbf{z} . (Right) Largest singular value of the Jacobian $\mathbf{J}_{\phi^{L-1}}(\mathbf{x} + \mathbf{z})$ as a function of the magnitude $\|\mathbf{z}\|_2$ of random and adversarial perturbations \mathbf{z} . The dashed vertical line indicates the ϵ used during adversarial training. Curves were aggregated over 200 samples from the test set. We can see that adversarially trained and data-dependent spectral norm regularized models are significantly more linear around data points than normally trained ones and that for AT and d.-d. SNR models, the Jacobian $\mathbf{J}_f(\mathbf{x})$ is a good approximation for the classifier in the entire ϵ -ball around \mathbf{x} .

linear than the clean trained one, both in random as well as adversarial directions. Compared to the normally trained model, the adversarially trained and spectral norm regularized ones remain flat in random directions for perturbations of considerable magnitude and even remain flat in the adversarial direction for perturbation magnitudes up to the order of the ϵ used during adversarial training, while the deviation from linearity seems to increase roughly linearly with $\|\mathbf{z}\|_2$ thereafter. The global spectral norm regularized model behaves similar to the normally trained one.

This means that for adversarially trained and data-dependent spectral norm regularized models, the Jacobian $\mathbf{J}_f(\mathbf{x})$ is a good approximation for the classifier in the entire ϵ -ball around \mathbf{x} , as the deviation from linearity is negligible for both random perturbations and adversarial perturbations of magnitude up to ϵ . In other words, the second order effects are negligible at that scale.

Largest singular value over distance. Figure 4 (right) shows the largest singular value of the linear operator $\mathbf{J}_{\phi^{L-1}}(\mathbf{x} + \mathbf{z})$ as the distance $\|\mathbf{z}\|_2$ from \mathbf{x} is increased, both along random and adversarial directions, for different training methods. We can see that the naturally trained network develops large dominant singular values around the data point during training, while the adversarially trained and data-dependent spectral norm regularized models manage to keep the dominant singular value low in the vicinity of \mathbf{x} .

5.5. Activation patterns

An important property of data-dependent operator norm regularization (and by our Theorem also adversarial training) is that it primarily acts on the data manifold whereas it should have comparatively little effect on irrelevant parts of the input space. We test this hypothesis empirically by com-

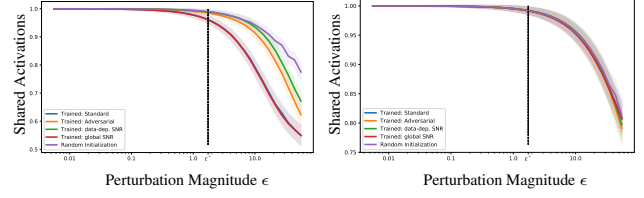


Figure 5. Fraction of shared activations as a function of noise magnitude ϵ between activation patterns $\phi_{(\cdot)}$ and $\phi_{(\cdot)+\mathbf{z}}$, where (\cdot) is either (left) a data point \mathbf{x} sampled from the test set, or (right) a data point \mathbf{n} sampled uniformly from the input domain (a.s. not on the data manifold) and \mathbf{z} is uniform noise of magnitude ϵ . For comparison, Figure 8 in the Appendix shows the fraction of shared activations under adversarial perturbations. We can see that both data-dependent SNR and adversarial training significantly increase the size of the ReLU cells in the input space around the data, but have no effect away from the data manifold.

paring activation patterns $\phi_{(\cdot)} \in \{0, 1\}^m$ of perturbed input samples under different regularization conditions, where m is the total number of activations in the network.

To this end, we measure the fraction of shared activations $m^{-1}(\phi_{(\cdot)} \cap \phi_{(\cdot)+\mathbf{z}})$, where (\cdot) is either a data point \mathbf{x} sampled from the test set, shown in Figure 5 (left), or a data point \mathbf{n} sampled uniformly from the input domain (a.s. not on the data manifold), shown in Figure 5 (right), and where \mathbf{z} is a random uniform noise vector of magnitude ϵ . From these curves, we can estimate the average size of the ReLU cells making up the activation pattern $\phi_{(\cdot)}$: The further to the right the line breaks away from 1.0, the longer the activation pattern stays constant, the larger the ReLU cells are around the input point. We can see two things: First, both data-dependent SNR and adversarial training significantly increase the size of the ReLU cells around the data manifold compared to a normally trained or globally regularized network. Second, data-dependent SNR and adversarial training have no effect on irrelevant parts of the input space, since off the data manifold, the ReLU cell size is not affected. This provides further evidence for the equivalence of data-dependent SNR and adversarial training as well as the qualitative differences between global and data-dependent regularization outlined in Section 5.4.

6. Conclusion

We established a theoretical link between adversarial training and operator norm regularization for deep neural networks. Specifically, we derive the precise conditions under which ℓ_p -norm constrained projected gradient ascent with an ℓ_q -norm loss on the logits of clean and perturbed inputs is equivalent to data-dependent (p, q) operator norm regularization. This fundamental connection confirms the long-standing argument that a network’s sensitivity to adversarial examples is tied to its spectral properties.

Acknowledgements

We would like to thank Michael Tschannen, Sebastian Nowozin and Antonio Orvieto for insightful discussions and helpful comments.

References

- Athalye, A., Carlini, N., and Wagner, D. Obfuscated gradients give a false sense of security: Circumventing defenses to adversarial examples. *arXiv preprint arXiv:1802.00420*, 2018.
- Bartlett, P. L., Foster, D. J., and Telgarsky, M. J. Spectrally-normalized margin bounds for neural networks. In *Advances in Neural Information Processing Systems*, pp. 6241–6250, 2017.
- Bertsimas, D. and Copenhaver, M. S. Characterization of the equivalence of robustification and regularization in linear and matrix regression. *European Journal of Operational Research*, 270(3):931–942, 2018.
- Bietti, A., Mialon, G., and Mairal, J. On regularization and robustness of deep neural networks. *arXiv preprint arXiv:1810.00363*, 2018.
- Biggio, B., Corona, I., Maiorca, D., Nelson, B., Srndic, N., Laskov, P., Giacinto, G., and Roli, F. Evasion attacks against machine learning at test time. In *Joint European conference on machine learning and knowledge discovery in databases*, pp. 387–402. Springer, 2013.
- Boyd, D. W. The power method for l_p norms. *Linear Algebra and its Applications*, 9:95–101, 1974.
- Bubeck, S., Price, E., and Razenshteyn, I. Adversarial examples from computational constraints. *arXiv preprint arXiv:1805.10204*, 2018.
- Carlini, N. and Wagner, D. Adversarial examples are not easily detected: Bypassing ten detection methods. In *Proceedings of the 10th ACM Workshop on Artificial Intelligence and Security*, pp. 3–14. ACM, 2017.
- Cisse, M., Bojanowski, P., Grave, E., Dauphin, Y., and Usunier, N. Parseval networks: Improving robustness to adversarial examples. In *International Conference on Machine Learning*, pp. 854–863, 2017.
- El Ghaoui, L. and Lebret, H. Robust solutions to least-squares problems with uncertain data. *SIAM Journal on matrix analysis and applications*, 18(4):1035–1064, 1997.
- Farnia, F., Zhang, J. M., and Tse, D. Generalizable adversarial training via spectral normalization. *arXiv preprint arXiv:1811.07457*, 2018.
- Fawzi, A., Fawzi, H., and Fawzi, O. Adversarial vulnerability for any classifier. *arXiv preprint arXiv:1802.08686*, 2018.
- Feinman, R., Curtin, R. R., Shintre, S., and Gardner, A. B. Detecting adversarial samples from artifacts. *arXiv preprint arXiv:1703.00410*, 2017.
- Gao, R. and Kleywegt, A. J. Distributionally robust stochastic optimization with wasserstein distance. *arXiv preprint arXiv:1604.02199*, 2016.
- Gilmer, J., Metz, L., Faghri, F., Schoenholz, S. S., Raghu, M., Wattenberg, M., and Goodfellow, I. Adversarial spheres. *arXiv preprint arXiv:1801.02774*, 2018.
- Goodfellow, I. J., Shlens, J., and Szegedy, C. Explaining and harnessing adversarial examples. *arXiv preprint arXiv:1412.6572*, 2014.
- Grosse, K., Manoharan, P., Papernot, N., Backes, M., and McDaniel, P. On the (statistical) detection of adversarial examples. *arXiv preprint arXiv:1702.06280*, 2017.
- Gu, S. and Rigazio, L. Towards deep neural network architectures robust to adversarial examples. *arXiv preprint arXiv:1412.5068*, 2014.
- Hein, M. and Andriushchenko, M. Formal guarantees on the robustness of a classifier against adversarial manipulation. In *Advances in Neural Information Processing Systems*, pp. 2266–2276, 2017.
- Higham, N. J. Estimating the matrix p -norm. *Numerische Mathematik*, 62(1):539–555, 1992.
- Hinton, G., Deng, L., Yu, D., Dahl, G. E., Mohamed, A.-r., Jaitly, N., Senior, A., Vanhoucke, V., Nguyen, P., Sainath, T. N., et al. Deep neural networks for acoustic modeling in speech recognition: The shared views of four research groups. *IEEE Signal Processing Magazine*, 29(6):82–97, 2012.
- Krizhevsky, A. and Hinton, G. Learning multiple layers of features from tiny images. 2009.
- Kurakin, A., Goodfellow, I., and Bengio, S. Adversarial examples in the physical world. *arXiv preprint arXiv:1607.02533*, 2016.
- LeCun, Y., Bengio, Y., and Hinton, G. Deep learning. *nature*, 521(7553):436, 2015.
- Lyu, C., Huang, K., and Liang, H.-N. A unified gradient regularization family for adversarial examples. In *2015 IEEE International Conference on Data Mining*, pp. 301–309. IEEE, 2015.

- Madry, A., Makelov, A., Schmidt, L., Tsipras, D., and Vladu, A. Towards deep learning models resistant to adversarial attacks. *arXiv preprint arXiv:1706.06083*, 2017.
- Metzen, J. H., Genewein, T., Fischer, V., and Bischoff, B. On detecting adversarial perturbations. *arXiv preprint arXiv:1702.04267*, 2017.
- Miyato, T., Maeda, S.-i., Koyama, M., Nakae, K., and Ishii, S. Distributional smoothing with virtual adversarial training. *arXiv preprint arXiv:1507.00677*, 2015.
- Miyato, T., Maeda, S.-i., Koyama, M., and Ishii, S. Virtual adversarial training: a regularization method for supervised and semi-supervised learning. *arXiv preprint arXiv:1704.03976*, 2017.
- Miyato, T., Kataoka, T., Koyama, M., and Yoshida, Y. Spectral normalization for generative adversarial networks. *arXiv preprint arXiv:1802.05957*, 2018.
- Moosavi-Dezfooli, S. M., Fawzi, A., and Frossard, P. Deepfool: a simple and accurate method to fool deep neural networks. In *Proceedings of 2016 IEEE Conference on Computer Vision and Pattern Recognition (CVPR)*, number EPFL-CONF-218057, 2016.
- Moosavi-Dezfooli, S.-M., Fawzi, A., Fawzi, O., and Frossard, P. Universal adversarial perturbations. *arXiv preprint*, 2017.
- Namkoong, H. and Duchi, J. C. Variance-based regularization with convex objectives. In *Advances in Neural Information Processing Systems*, pp. 2975–2984, 2017.
- Neyshabur, B., Tomioka, R., and Srebro, N. Norm-based capacity control in neural networks. In *Conference on Learning Theory*, pp. 1376–1401, 2015.
- Novak, R., Bahri, Y., Abolafia, D. A., Pennington, J., and Sohl-Dickstein, J. Sensitivity and generalization in neural networks: an empirical study. *arXiv preprint arXiv:1802.08760*, 2018.
- Papernot, N., McDaniel, P., and Goodfellow, I. Transferability in machine learning: from phenomena to black-box attacks using adversarial samples. *arXiv preprint arXiv:1605.07277*, 2016.
- Papernot, N., Carlini, N., Goodfellow, I., Feinman, R., Faghri, F., Matyasko, A., Hambardzumyan, K., Juang, Y.-L., Kurakin, A., Sheatsley, R., Garg, A., and Lin, Y.-C. cleverhans v2.0.0: an adversarial machine learning library. *arXiv preprint arXiv:1610.00768*, 2017.
- Raghu, M., Poole, B., Kleinberg, J., Ganguli, S., and Dickstein, J. S. On the expressive power of deep neural networks. In *Proceedings of the 34th International Conference on Machine Learning-Volume 70*, pp. 2847–2854. JMLR. org, 2017.
- Raghunathan, A., Steinhardt, J., and Liang, P. Certified defenses against adversarial examples. *arXiv preprint arXiv:1801.09344*, 2018.
- Roth, K., Kilcher, Y., and Hofmann, T. The odds are odd: A statistical test for detecting adversarial examples. *arXiv preprint arXiv:1902.04818*, 2019.
- Sabour, S., Cao, Y., Faghri, F., and Fleet, D. J. Adversarial manipulation of deep representations. *arXiv preprint arXiv:1511.05122*, 2015.
- Schmidt, L., Santurkar, S., Tsipras, D., Talwar, K., and Madry, A. Adversarially robust generalization requires more data. *arXiv preprint arXiv:1804.11285*, 2018.
- Shaham, U., Yamada, Y., and Negahban, S. Understanding adversarial training: Increasing local stability of neural nets through robust optimization. *arXiv preprint arXiv:1511.05432*, 2015.
- Simonyan, K. and Zisserman, A. Very deep convolutional networks for large-scale image recognition. In *International Conference on Learning Representations (ICLR)*, 2014.
- Sinha, A., Namkoong, H., and Duchi, J. Certifiable distributional robustness with principled adversarial training. *arXiv preprint arXiv:1710.10571*, 2017.
- Szegedy, C., Zaremba, W., Sutskever, I., Bruna, J., Erhan, D., Goodfellow, I., and Fergus, R. Intriguing properties of neural networks. *arXiv preprint arXiv:1312.6199*, 2013.
- Tropp, J. A. *Topics in sparse approximation*. PhD thesis, 2004.
- Tsuzuku, Y., Sato, I., and Sugiyama, M. Lipschitz-margin training: Scalable certification of perturbation invariance for deep neural networks. In *Advances in Neural Information Processing Systems*, pp. 6541–6550, 2018.
- Wong, E., Schmidt, F. R., and Kolter, J. Z. Wasserstein adversarial examples via projected sinkhorn iterations. *arXiv preprint arXiv:1902.07906*, 2019.
- Xu, H., Caramanis, C., and Mannor, S. Robustness and regularization of support vector machines. *Journal of Machine Learning Research*, 10(Jul):1485–1510, 2009.
- Xu, W., Evans, D., and Qi, Y. Feature squeezing: Detecting adversarial examples in deep neural networks. *arXiv preprint arXiv:1704.01155*, 2017.

Yoshida, Y. and Miyato, T. Spectral norm regularization for improving the generalizability of deep learning. *arXiv preprint arXiv:1705.10941*, 2017.

Zagoruyko, S. and Komodakis, N. Wide residual networks. *arXiv preprint arXiv:1605.07146*, 2016.

7. Appendix

The proof of the main Theorem can be found in Sections 7.3 & 7.4. Additional implementation details can be found in Sections 7.7-7.9. Additional experimental results are presented in Sections 7.10-7.14. We begin with a short recap on robust optimization in linear regression and a derivation of the optimal perturbation to a linear function under a norm constraint.

7.1. Recap: Robust Optimization and Regularization for Linear Regression

In this section, we recapitulate the basic ideas on the relation between robust optimization and regularization presented in (Bertsimas & Copenhaver, 2018). Note that the notation deviates slightly from the main text: most importantly, the perturbations Δ refer to perturbations of the entire training data \mathbf{X} , as is common in robust optimization.

Consider linear regression with additive perturbations Δ of the data matrix \mathbf{X}

$$\min_{\mathbf{w}} \max_{\Delta \in \mathcal{U}} h(\mathbf{y} - (\mathbf{X} + \Delta)\mathbf{w}), \quad (25)$$

where $h : \mathbb{R}^n \rightarrow \mathbb{R}$ denotes a loss function and \mathcal{U} denotes the uncertainty set. A general way to construct \mathcal{U} is as a ball of bounded matrix norm perturbations $\mathcal{U} = \{\Delta : \|\Delta\| \leq \lambda\}$. Of particular interest are induced matrix norms

$$\|\mathbf{A}\|_{g,h} := \max_{\mathbf{w}} \left\{ \frac{h(\mathbf{A}\mathbf{w})}{g(\mathbf{w})} \right\}, \quad (26)$$

where $h : \mathbb{R}^n \rightarrow \mathbb{R}$ is a semi-norm and $g : \mathbb{R}^d \rightarrow \mathbb{R}$ is a norm. It is obvious that if h fulfills the triangle inequality then one can upper bound

$$\begin{aligned} h(\mathbf{y} - (\mathbf{X} + \Delta)\mathbf{w}) &\leq h(\mathbf{y} - \mathbf{X}\mathbf{w}) + h(\Delta\mathbf{w}) \\ &\leq h(\mathbf{y} - \mathbf{X}\mathbf{w}) + \lambda g(\mathbf{w}), \quad \forall \Delta \in \mathcal{U}, \end{aligned} \quad (27)$$

by using (a) the triangle inequality and (b) the definition of the matrix norm.

The question then is, under which circumstances both inequalities become equalities at the maximizing Δ^* . It is straightforward to check (Bertsimas & Copenhaver, 2018) Theorem 1 that specifically we may choose the rank 1 matrix

$$\Delta^* = \frac{\lambda}{h(\mathbf{r})} \mathbf{r}\mathbf{v}^\top, \quad (28)$$

where

$$\mathbf{r} = \mathbf{y} - \mathbf{X}\mathbf{w}, \quad \mathbf{v} = \arg \max_{\mathbf{v}: g^*(\mathbf{v})=1} \{\mathbf{v}^\top \mathbf{w}\}, \quad (29)$$

with g^* as the dual norm. If $h(\mathbf{r}) = 0$ then one can pick any \mathbf{u} for which $h(\mathbf{u}) = 1$ to form $\Delta = \lambda \mathbf{u}\mathbf{v}^\top$ (such a \mathbf{u} has to exist if h is not identically zero). This shows that, for robust linear regression with induced matrix norm uncertainty sets, robust optimization is equivalent to regularization.

7.2. Optimal Perturbation to Linear Function

Lemma 1 (Optimal Perturbation). *Explicit expression for the optimal perturbation to a linear function under an ℓ_p -norm constraint⁶. Let \mathbf{z} be an arbitrary non-zero vector, e.g. $\mathbf{z} = \nabla_{\mathbf{x}} \ell_{\text{adv}}$, and let \mathbf{v} be a vector of the same dimension. Then,*

$$\mathbf{v}^* = \arg \max_{\mathbf{v}: \|\mathbf{v}\|_p \leq 1} \mathbf{v}^\top \mathbf{z} = \frac{\text{sign}(\mathbf{z}) \odot |\mathbf{z}|^{p^*-1}}{\|\mathbf{z}\|_{p^*}^{p^*-1}} \quad (30)$$

where \odot , $\text{sign}(\cdot)$ and $|\cdot|$ denote elementwise product, sign and absolute value, and p^* is the Hölder conjugate of p , given by $1/p + 1/p^* = 1$. Note that the maximizer \mathbf{v}^* is attained at a \mathbf{v} with $\|\mathbf{v}\|_p = 1$, since $\mathbf{v}^\top \mathbf{z}$ is linear in \mathbf{v} .

In particular, we have the following special cases, which is also how the Projected Gradient Descent attack is implemented in the cleverhans library (Papernot et al., 2017),

$$\arg \max_{\mathbf{v}: \|\mathbf{v}\|_p \leq 1} \mathbf{v}^\top \mathbf{z} = \begin{cases} \mathbf{z}/\|\mathbf{z}\|_2 & \text{for } p = 2 \\ \text{sign}(\mathbf{z}) & \text{for } p = \infty \\ \frac{1}{|\mathcal{I}|} \text{sign}(\mathbf{z}) \odot \mathbf{1}_{\mathcal{I}} & \text{for } p = 1 \end{cases} \quad (31)$$

The optimal ℓ_1 -norm constrained perturbation can be taken to be $\lim_{p^* \rightarrow \infty} \text{sign}(\mathbf{z}) \odot |\mathbf{z}|^{p^*-1} / \|\mathbf{z}\|_{p^*}^{p^*-1} = |\mathcal{I}|^{-1} \text{sign}(\mathbf{z}) \odot \mathbf{1}_{\mathcal{I}}$ with $\mathbf{1}_{\mathcal{I}} = \sum_{i \in \mathcal{I}} \mathbf{e}_i$, where $\mathcal{I} := \{j \in [1, \dots, n] : |z_j| = \|\mathbf{z}\|_\infty\}$ denotes the set of indices at which \mathbf{z} attains its maximum norm, and \mathbf{e}_i is the i -th canonical unit-vector. Note that any other convex combination of unit-vectors from the set of indices at which \mathbf{z} attains its maximum absolute value is also a valid optimal ℓ_1 -norm constrained perturbation.

Finally, before we continue with the proof, we would like to note that the above expression for the maximizer has already been stated in the DeepFool paper (Moosavi Dezfooli et al., 2016), although it hasn't been derived there.

Proof. By Hölder's inequality, we have for non-zero \mathbf{z} ,

$$\mathbf{v}^\top \mathbf{z} \leq \|\mathbf{v}\|_p \|\mathbf{z}\|_{p^*}, \quad \text{w. equality iff } |\mathbf{v}|^p = \gamma |\mathbf{z}|^{p^*} \quad (32)$$

i.e. equality⁷ holds if and only if $|\mathbf{v}|^p$ and $|\mathbf{z}|^{p^*}$ are linearly dependent, where $|\cdot|$ denotes elementwise absolute-value, and where p^* is given by $1/p + 1/p^* = 1$. The proportionality constant γ is determined by the normalization require-

⁶Note that for $p \in \{1, \infty\}$ the maximizer might not be unique, in which case we simply choose a specific representative.

⁷Note that technically equality only holds for $p, p^* \in (1, \infty)$. But one can easily check that the explicit expressions for $p \in \{1, \infty\}$ are in fact optimal. See comment after Equation 1.1 in (Higham, 1992).

ment $\|\mathbf{v}\|_p = 1$. For $1 < p < \infty$, we have

$$\|\mathbf{v}\|_p = \left(\gamma \sum_{i=1}^n |z_i|^{p^*}\right)^{1/p} \stackrel{!}{=} 1 \implies \gamma = \|\mathbf{z}\|_{p^*}^{-p^*} \quad (33)$$

Thus, equality holds iff $|\mathbf{v}| = |\mathbf{z}|^{p^*/p} / \|\mathbf{z}\|_{p^*}^{p^*/p}$, which implies that $\mathbf{v}^* = \text{sign}(\mathbf{z}) \odot |\mathbf{z}|^{p^*-1} / \|\mathbf{z}\|_{p^*}^{p^*-1}$, since \mathbf{v} must have the same sign as \mathbf{z} and $p^*/p = p^* - 1$. For $p = 1$, $\gamma = (|\mathcal{I}| \|\mathbf{z}\|_\infty)^{-1}$, where $\mathcal{I} := \{j \in [1, \dots, n] : |z_j| = \|\mathbf{z}\|_\infty\}$, i.e. $|\mathcal{I}|$ counts the multiplicity of the maximum element in the maximum norm. It is easy to see that $|\mathcal{I}|^{-1} \text{sign}(\mathbf{z}) \odot \mathbf{1}_{\mathcal{I}}$ is a maximizer in this case. For $p = \infty$, it is trivially clear that the maximizer \mathbf{v}^* is given by $\text{sign}(\mathbf{z})$. \square

As an illustrative sanity-check, let us also verify that the above explicit expression for the optimal perturbation \mathbf{v}^* has ℓ_p norm equal to one. Let \mathbf{z} be an arbitrary non-zero vector of the same dimension as \mathbf{v} and let $1 < p < \infty$, then

$$\|\mathbf{v}^*\|_p = \left(\sum_{i=1}^n \left| \frac{\text{sign}(z_i) |z_i|^{p^*-1}}{\|\mathbf{z}\|_{p^*}^{p^*-1}} \right|^p\right)^{1/p} \quad (34)$$

$$= \left(\sum_{i=1}^n \left(\frac{|z_i|^{p^*-1}}{\|\mathbf{z}\|_{p^*}^{p^*-1}}\right)^p\right)^{1/p} \quad (35)$$

$$= \left(\sum_{i=1}^n \frac{|z_i|^{p^*}}{\|\mathbf{z}\|_{p^*}^{p^*}}\right)^{1/p} = 1 \quad (36)$$

where we have used that $(p^* - 1)p = p^*$. For $p = 1$, we have

$$\|\mathbf{v}^*\|_1 = \sum_{i=1}^n \left| \frac{1}{|\mathcal{I}|} \text{sign}(z_i) \mathbf{1}_{\{i \in \mathcal{I}\}} \right| \quad (37)$$

$$= \sum_{i=1}^n \left| \frac{1}{|\mathcal{I}|} \mathbf{1}_{\{i \in \mathcal{I}\}} \right| = 1 \quad (38)$$

where $\mathbf{1}_{\{\cdot\}}$ denotes the indicator function. For $p = \infty$, we have

$$\|\mathbf{v}^*\|_\infty = \max_i |\text{sign}(z_i)| = 1 \quad (39)$$

7.3. Projection Lemma

In this section, we prove the following intuitive Lemma.

Lemma 2 (Projection Lemma). *(First part) Let \mathbf{v} and $\tilde{\mathbf{v}} \neq \mathbf{0}$ be two arbitrary (non-zero) vectors of the same dimension. Then*

$$\lim_{\alpha \rightarrow \infty} \Pi_{\{\|\cdot\|_p=1\}}(\mathbf{v} + \alpha \tilde{\mathbf{v}}) = \frac{\text{sign}(\tilde{\mathbf{v}}) \odot |\tilde{\mathbf{v}}|^{p^*-1}}{\|\tilde{\mathbf{v}}\|_{p^*}^{p^*-1}} \quad (40)$$

where \odot , $\text{sign}(\cdot)$ and $|\cdot|$ denote elementwise product, sign and absolute-value, and where p^* denotes the Hölder conjugate of p defined by $1/p + 1/p^* = 1$. Moreover, if

$\tilde{\mathbf{v}}$ is of the form $\tilde{\mathbf{v}} = \text{sign}(\mathbf{z}) \odot |\mathbf{z}|^{p^*-1} / \|\mathbf{z}\|_{p^*}^{p^*-1}$, for an arbitrary non-zero vector \mathbf{z} and $p \in \{1, 2, \infty\}$, then $\lim_{\alpha \rightarrow \infty} \Pi_{\{\|\cdot\|_p=1\}}(\mathbf{v} + \alpha \tilde{\mathbf{v}}) = \tilde{\mathbf{v}}$. (Second part) Let $\mathbf{x}_{k-1} \in \mathcal{B}_\epsilon^p(\mathbf{x})$ and let $\mathbf{v}_k \neq \mathbf{0}$ be an arbitrary non-zero vector of the same dimension. Then

$$\mathbf{x}_k = \lim_{\alpha \rightarrow \infty} \Pi_{\mathcal{B}_\epsilon^p(\mathbf{x})}(\mathbf{x}_{k-1} + \alpha \mathbf{v}_k) \quad (41)$$

$$= \mathbf{x} + \lim_{\alpha \rightarrow \infty} \Pi_{\{\|\cdot\|_p=\epsilon\}}(\alpha \mathbf{v}_k) \quad (42)$$

$$= \mathbf{x} + \epsilon \frac{\text{sign}(\mathbf{v}_k) \odot |\mathbf{v}_k|^{p^*-1}}{\|\mathbf{v}_k\|_{p^*}^{p^*-1}} \quad (43)$$

Moreover, if \mathbf{v}_k is of the form $\mathbf{v}_k = \text{sign}(\mathbf{z}) \odot |\mathbf{z}|^{p^*-1} / \|\mathbf{z}\|_{p^*}^{p^*-1}$, for $p \in \{1, 2, \infty\}$ and an arbitrary non-zero vector \mathbf{z} (as is the case if \mathbf{v}_k is given by the backward pass in Equation 23), then $\mathbf{x}_k = \mathbf{x} + \epsilon \mathbf{v}_k$.

Proof. First part.

$$\lim_{\alpha \rightarrow \infty} \Pi_{\{\|\cdot\|_p=1\}}(\mathbf{v} + \alpha \tilde{\mathbf{v}}) \quad (44)$$

$$= \lim_{\alpha \rightarrow \infty} \arg \min_{\mathbf{v}^*: \|\mathbf{v}^*\|_p=1} \|\mathbf{v}^* - \tilde{\mathbf{v}}\|_2 \quad (45)$$

$$= \lim_{\alpha \rightarrow \infty} \arg \min_{\mathbf{v}^*: \|\mathbf{v}^*\|_p=1} (\mathbf{v}^* - \tilde{\mathbf{v}})^\top (\mathbf{v}^* - \tilde{\mathbf{v}}) \quad (46)$$

$$= \lim_{\alpha \rightarrow \infty} \arg \min_{\mathbf{v}^*: \|\mathbf{v}^*\|_p=1} \mathbf{v}^{*\top} \mathbf{v}^* - 2\alpha \mathbf{v}^{*\top} \tilde{\mathbf{v}} + \text{const} \quad (47)$$

where the const term is independent of \mathbf{v}^* and thus irrelevant for the $\arg \min$. Next, we observe that in the limit $\alpha \rightarrow \infty$, the $\mathbf{v}^{*\top} \mathbf{v}^*$ term vanishes relative to the $\alpha \mathbf{v}^{*\top} \tilde{\mathbf{v}}$ term, hence

$$\lim_{\alpha \rightarrow \infty} \Pi_{\{\|\cdot\|_p=1\}}(\mathbf{v} + \alpha \tilde{\mathbf{v}}) \quad (48)$$

$$= \arg \min_{\mathbf{v}^*: \|\mathbf{v}^*\|_p=1} -\mathbf{v}^{*\top} \tilde{\mathbf{v}} \quad (49)$$

$$= \arg \max_{\mathbf{v}^*: \|\mathbf{v}^*\|_p=1} \mathbf{v}^{*\top} \tilde{\mathbf{v}} \quad (50)$$

$$= \frac{\text{sign}(\tilde{\mathbf{v}}) \odot |\tilde{\mathbf{v}}|^{p^*-1}}{\|\tilde{\mathbf{v}}\|_{p^*}^{p^*-1}} \quad (51)$$

where in the last line we have used Equation 20 for the optimal perturbation to a linear function under an ℓ_p -norm constraint that we have proven in Lemma 1.

Moreover, if $\tilde{\mathbf{v}}$ is of the form $\tilde{\mathbf{v}} = \text{sign}(\mathbf{z}) \odot |\mathbf{z}|^{p^*-1} / \|\mathbf{z}\|_{p^*}^{p^*-1}$, then

$$\frac{\text{sign}(\tilde{\mathbf{v}}) \odot |\tilde{\mathbf{v}}|^{p^*-1}}{\|\tilde{\mathbf{v}}\|_{p^*}^{p^*-1}} = \frac{\text{sign}(\mathbf{z}) \odot |\mathbf{z}|^{(p^*-1)(p^*-1)}}{\|\mathbf{z}\|_{p^*}^{p^*-1} \|\mathbf{z}\|_{p^*}^{p^*-1}} \quad (52)$$

Now, observe that for $p \in \{1, 2, \infty\}$, the Hölder conjugate $p^* \in \{1, 2, \infty\}$. In particular, for these values p^* satisfies $(p^*-1)(p^*-1) = p^*-1$ (since $0 \cdot 0 = 0, 1 \cdot 1 = 1, \infty \cdot \infty = \infty$).

Thus, the numerator (and hence the direction) remains the same. Moreover, we also have that $\| |z|^{p^*-1} \|_{p^*}^{p^*-1} = \|z\|_{p^*}^{p^*-1}$ (and hence the magnitude remains the same, too). For $p^* = 1$, $\| |z|^0 \|_1^0 = \|1\|_1^0 = 1 = \|z\|_1^0$ for any non-zero z . For $p^* = 2$, $\| |z|^1 \|_2^1 = \|z\|_2$ for any z . For the $p^* = \infty$ case, we consider the full expression $\text{sign}(z) \odot |z|^{(p^*-1)/(p^*-1)} / \| |z|^{p^*-1} \|_{p^*}^{p^*-1} = |\mathcal{I}'|^{-1} \text{sign}(z) \odot \mathbf{1}_{\mathcal{I}'}$ where $\mathcal{I}' := \{j \in [1, \dots, n] : |z_j|^{p^*-1} = \| |z|^{p^*-1} \|_{\infty}\}$ denotes the set of indices at which $|z|^{p^*-1}$ attains its maximum norm. It is easy to see that $\mathcal{I}' = \mathcal{I}$, i.e. the set of indices of maximal elements remains the same.

Thus, if $\tilde{\mathbf{v}}$ is of the form $\tilde{\mathbf{v}} = \text{sign}(z) \odot |z|^{p^*-1} / \| |z|^{p^*-1} \|_{p^*}^{p^*-1}$, then it is a fix point of Equation 20 and hence of the projection $\lim_{\alpha \rightarrow \infty} \Pi_{\{\|\cdot\|_p=1\}}(\mathbf{v} + \alpha\tilde{\mathbf{v}})$,

$$\frac{\text{sign}(\tilde{\mathbf{v}}) \odot |\tilde{\mathbf{v}}|^{p^*-1}}{\|\tilde{\mathbf{v}}\|_{p^*}^{p^*-1}} = \tilde{\mathbf{v}} \text{ for } p^* \in \{1, 2, \infty\} \quad (53)$$

Another way to see this is by checking that the operation $\text{sign}(\cdot) \odot |\cdot|^{p^*-1} / \|\cdot\|_{p^*}^{p^*-1}$, for $p^* \in \{1, 2, \infty\}$, leaves the corresponding explicit expressions for the optimal perturbation in the RHS of Equation 31 invariant.

Finally, note how the Projection Lemma implies that $\arg \max_{\mathbf{v}: \|\mathbf{v}\|_p \leq 1} \mathbf{v}^\top \mathbf{z} = \lim_{\alpha \rightarrow \infty} \Pi_{\{\|\cdot\|_p=1\}}(\alpha \mathbf{z})$, which is another interesting result in its own right.

Second part.

By definition of the orthogonal projection, we have

$$\mathbf{x}_k = \lim_{\alpha \rightarrow \infty} \Pi_{\mathcal{B}_\epsilon^p(\mathbf{x})}(\mathbf{x}_{k-1} + \alpha \mathbf{v}_k) \quad (54)$$

$$= \lim_{\alpha \rightarrow \infty} \arg \min_{\mathbf{x}^*: \|\mathbf{x}^* - \mathbf{x}\|_p \leq \epsilon} \|\mathbf{x}^* - \mathbf{x}_{k-1} - \alpha \mathbf{v}_k\|_2 \quad (55)$$

$$= \lim_{\alpha \rightarrow \infty} \arg \min_{\mathbf{x} + \mathbf{v}^*: \|\mathbf{v}^*\|_p \leq \epsilon} \|\mathbf{x} + \mathbf{v}^* - \mathbf{x}_{k-1} - \alpha \mathbf{v}_k\|_2 \quad (56)$$

$$= \mathbf{x} + \lim_{\alpha \rightarrow \infty} \arg \min_{\mathbf{v}^*: \|\mathbf{v}^*\|_p \leq \epsilon} \|\mathbf{x} + \mathbf{v}^* - \mathbf{x}_{k-1} - \alpha \mathbf{v}_k\|_2^2 \quad (57)$$

$$= \mathbf{x} + \lim_{\alpha \rightarrow \infty} \arg \min_{\mathbf{v}^*: \|\mathbf{v}^*\|_p \leq \epsilon} \left\{ \|\mathbf{v}^* - \alpha \mathbf{v}_k\|_2^2 + 2\mathbf{v}^{*\top} \text{const} + \text{const}^2 \right\} \quad (58)$$

$$= \mathbf{x} + \lim_{\alpha \rightarrow \infty} \arg \min_{\mathbf{v}^*: \|\mathbf{v}^*\|_p \leq \epsilon} \|\mathbf{v}^* - \alpha \mathbf{v}_k\|_2^2 \quad (59)$$

$$= \mathbf{x} + \lim_{\alpha \rightarrow \infty} \arg \min_{\mathbf{v}^*: \|\mathbf{v}^*\|_p \leq \epsilon} \|\mathbf{v}^* - \alpha \mathbf{v}_k\|_2 \quad (60)$$

$$= \mathbf{x} + \lim_{\alpha \rightarrow \infty} \arg \min_{\mathbf{v}^*: \|\mathbf{v}^*\|_p = \epsilon} \|\mathbf{v}^* - \alpha \mathbf{v}_k\|_2 \quad (61)$$

$$= \mathbf{x} + \lim_{\alpha \rightarrow \infty} \Pi_{\{\|\cdot\|_p=\epsilon\}}(\alpha \mathbf{v}_k) \quad (62)$$

where (i) we have used that the const term is independent of \mathbf{v}^* and thus irrelevant for the arg min, (ii) in the fourth-to-last line we have dropped all the terms that vanish relative

to the limit $\alpha \rightarrow \infty$, and (iii) since $\alpha \mathbf{v}_k$ is outside the ℓ_p -ball in the limit $\alpha \rightarrow \infty$, projecting into the ℓ_p -ball $\{\mathbf{v}^* : \|\mathbf{v}^*\|_p \leq 1\}$ is equivalent to projecting onto its boundary $\{\mathbf{v}^* : \|\mathbf{v}^*\|_p = 1\}$.

By the first part of the Projection Lemma, we also have that

$$\mathbf{x}_k = \mathbf{x} + \lim_{\alpha \rightarrow \infty} \Pi_{\{\|\cdot\|_p=\epsilon\}}(\alpha \mathbf{v}_k) \quad (63)$$

$$= \mathbf{x} + \epsilon \frac{\text{sign}(\mathbf{v}_k) \odot |\mathbf{v}_k|^{p^*-1}}{\|\mathbf{v}_k\|_{p^*}^{p^*-1}} \quad (64)$$

$$= \mathbf{x} + \epsilon \mathbf{v}_k \quad \text{if } \mathbf{v}_k = \frac{\text{sign}(z) \odot |z|^{p^*-1}}{\|z\|_{p^*}^{p^*-1}} \quad (65)$$

for an arbitrary non-zero vector z . This completes the proof of the Lemma.

For illustrative purposes, we provide an alternative proof of the second part of the Lemma for $p \in \{2, \infty\}$, because for these values the projection can be written down explicitly away from the $\alpha \rightarrow \infty$ limit (the $p = 1$ projection can be written down in a simple form in the $\alpha \rightarrow \infty$ limit only).

We first consider the case $p = 2$. The ℓ_2 -norm ball projection can be expressed as follows,

$$\Pi_{\mathcal{B}_\epsilon^2(\mathbf{x})}(\tilde{\mathbf{x}}_k) = \mathbf{x} + \epsilon(\tilde{\mathbf{x}}_k - \mathbf{x}) / \max(\epsilon, \|\tilde{\mathbf{x}}_k - \mathbf{x}\|_2), \quad (66)$$

where $\tilde{\mathbf{x}}_k = \mathbf{x}_{k-1} + \alpha \mathbf{v}_k$ and where the $\max(\epsilon, \|\tilde{\mathbf{x}}_k - \mathbf{x}\|_2)$ ensures that if $\|\tilde{\mathbf{x}}_k - \mathbf{x}\|_2 < \epsilon$ then $\mathbf{x}_k = \tilde{\mathbf{x}}_k$, i.e. we only need to project $\tilde{\mathbf{x}}_k$ if it is outside the ϵ -ball $\mathcal{B}_\epsilon^2(\mathbf{x})$.

Thus, in the limit $\alpha \rightarrow \infty$,

$$\lim_{\alpha \rightarrow \infty} \Pi_{\mathcal{B}_\epsilon^2(\mathbf{x})}(\mathbf{x}_{k-1} + \alpha \mathbf{v}_k) \quad (67)$$

$$= \lim_{\alpha \rightarrow \infty} \mathbf{x} + \epsilon \frac{\tilde{\mathbf{x}}_k - \mathbf{x}}{\max(\epsilon, \|\tilde{\mathbf{x}}_k - \mathbf{x}\|_2)} \quad (68)$$

$$= \mathbf{x} + \epsilon \lim_{\alpha \rightarrow \infty} \frac{\mathbf{x}_{k-1} + \alpha \mathbf{v}_k - \mathbf{x}}{\max(\epsilon, \|\mathbf{x}_{k-1} + \alpha \mathbf{v}_k - \mathbf{x}\|_2)} \quad (69)$$

$$= \mathbf{x} + \epsilon \lim_{\alpha \rightarrow \infty} \frac{\alpha(\mathbf{v}_k + \frac{1}{\alpha}(\mathbf{x}_{k-1} - \mathbf{x}))}{\max(\epsilon, \alpha \|\mathbf{v}_k + \frac{1}{\alpha}(\mathbf{x}_{k-1} - \mathbf{x})\|_2)} \quad (70)$$

$$= \mathbf{x} + \epsilon \lim_{\alpha \rightarrow \infty} \frac{\alpha(\mathbf{v}_k + \frac{1}{\alpha}(\mathbf{x}_{k-1} - \mathbf{x}))}{\alpha \|\mathbf{v}_k + \frac{1}{\alpha}(\mathbf{x}_{k-1} - \mathbf{x})\|_2} \quad (71)$$

$$= \mathbf{x} + \epsilon \lim_{\alpha \rightarrow \infty} \Pi_{\{\|\cdot\|_2=1\}}(\alpha \mathbf{v}_k) \quad (72)$$

$$= \mathbf{x} + \epsilon \mathbf{v}_k / \|\mathbf{v}_k\|_2 \quad (73)$$

$$= \mathbf{x} + \epsilon \mathbf{v}_k \quad \text{if } \mathbf{v}_k = \tilde{\mathbf{v}}_k / \|\tilde{\mathbf{v}}_k\|_2 \quad (74)$$

where in the fourth-to-last line we used that the max will be attained at its second argument in the limit $\alpha \rightarrow \infty$ since $\|\mathbf{v}_k + \frac{1}{\alpha}(\mathbf{x}_{k-1} - \mathbf{x})\|_2 > 0$ for $\mathbf{v}_k \neq 0$, and the last line holds if \mathbf{v}_k is of the form $\tilde{\mathbf{v}}_k / \|\tilde{\mathbf{v}}_k\|_2$.

Next, we consider the case $p = \infty$. The ℓ_∞ -norm ball projection (clipping) can be expressed as follows,

$$\Pi_{\mathcal{B}_\epsilon^\infty(\mathbf{x})}(\tilde{\mathbf{x}}_k) = \mathbf{x} + \max(-\epsilon, \min(\epsilon, \tilde{\mathbf{x}}_k - \mathbf{x})), \quad (75)$$

where $\tilde{\mathbf{x}}_k = \mathbf{x}_{k-1} + \alpha \mathbf{v}_k$ and where the max and min are taken *elementwise*. Note that the order of the max and min operators can be exchanged, as we prove in the ‘‘min-max-commutativity’’ Lemma 3 below.

Thus, in the limit $\alpha \rightarrow \infty$,

$$\lim_{\alpha \rightarrow \infty} \Pi_{\mathcal{B}_\epsilon^\infty(\mathbf{x})}(\mathbf{x}_{k-1} + \alpha \mathbf{v}_k) - \mathbf{x} \quad (76)$$

$$= \lim_{\alpha \rightarrow \infty} \max(-\epsilon, \min(\epsilon, \alpha \mathbf{v}_k + \mathbf{x}_{k-1} - \mathbf{x})) \quad (77)$$

$$= \lim_{\alpha \rightarrow \infty} \left\{ \mathbb{1}_{\{\text{sign}(\mathbf{v}_k) > 0\}} \max(-\epsilon, \min(\epsilon, \alpha |\mathbf{v}_k| + \mathbf{x}_{k-1} - \mathbf{x})) \right. \\ \left. + \mathbb{1}_{\{\text{sign}(\mathbf{v}_k) < 0\}} \max(-\epsilon, \min(\epsilon, -\alpha |\mathbf{v}_k| + \mathbf{x}_{k-1} - \mathbf{x})) \right\} \quad (78)$$

where in going from the second to the third line we used that $\mathbf{v}_k = \text{sign}(\mathbf{v}_k) \odot |\mathbf{v}_k|$.

Next, observe that

$$\lim_{\alpha \rightarrow \infty} \max(-\epsilon, \min(\epsilon, \alpha |\mathbf{v}_k| + \mathbf{x}_{k-1} - \mathbf{x})) \quad (79)$$

$$= \lim_{\alpha \rightarrow \infty} \min(\epsilon, \alpha |\mathbf{v}_k| + \mathbf{x}_{k-1} - \mathbf{x}) = \epsilon \quad (80)$$

since $\min(\epsilon, \alpha |\mathbf{v}_k| + \mathbf{x}_{k-1} - \mathbf{x}) > -\epsilon$.

Similarly, we have

$$\lim_{\alpha \rightarrow \infty} \max(-\epsilon, \min(\epsilon, -\alpha |\mathbf{v}_k| + \mathbf{x}_{k-1} - \mathbf{x})) \quad (81)$$

$$= \lim_{\alpha \rightarrow \infty} \min(\epsilon, \max(-\epsilon, -\alpha |\mathbf{v}_k| + \mathbf{x}_{k-1} - \mathbf{x})) \quad (82)$$

$$= \lim_{\alpha \rightarrow \infty} \max(-\epsilon, -\alpha |\mathbf{v}_k| + \mathbf{x}_{k-1} - \mathbf{x}) \quad (83)$$

$$= -\epsilon \quad (84)$$

where for the first equality we have used the ‘‘min-max-commutativity’’ Lemma 3 below, which asserts that the order of the max and min can be exchanged, while the second equality holds since $\max(-\epsilon, -\alpha |\mathbf{v}_k| + \mathbf{x}_{k-1} - \mathbf{x}) < \epsilon$.

With that, we can continue

$$\lim_{\alpha \rightarrow \infty} \Pi_{\mathcal{B}_\epsilon^\infty(\mathbf{x})}(\mathbf{x}_{k-1} + \alpha \mathbf{v}_k) \quad (85)$$

$$= \mathbf{x} + \epsilon \mathbb{1}_{\{\text{sign}(\mathbf{v}_k) > 0\}} - \epsilon \mathbb{1}_{\{\text{sign}(\mathbf{v}_k) < 0\}} \quad (86)$$

$$= \mathbf{x} + \epsilon \text{sign}(\mathbf{v}_k) \quad (87)$$

$$= \mathbf{x} + \epsilon \lim_{\alpha \rightarrow \infty} \Pi_{\{\|\cdot\|_\infty=1\}}(\alpha \mathbf{v}_k) \quad (88)$$

$$= \mathbf{x} + \epsilon \mathbf{v}_k \text{ if } \mathbf{v}_k = \text{sign}(\tilde{\mathbf{v}}_k) \quad (89)$$

where the last line holds if \mathbf{v}_k is of the form $\text{sign}(\mathbf{z})$, since in that case $\text{sign}(\mathbf{v}_k) = \text{sign}(\text{sign}(\tilde{\mathbf{v}}_k)) = \text{sign}(\tilde{\mathbf{v}}_k) = \mathbf{v}_k$.

Note that the last line can directly be obtained from the third-to-last line if $\mathbf{v}_k = \text{sign}(\tilde{\mathbf{v}}_k)$.

Finally, for the **general case**, we provide the following additional intuition. Taking the limit $\alpha \rightarrow \infty$ has two effects: firstly, it puts all the weight in the sum $\mathbf{x}_{k-1} + \alpha \mathbf{v}_k$ on $\alpha \mathbf{v}_k$ and secondly, it takes every component of \mathbf{v}_k out of the ϵ -ball $\mathcal{B}_\epsilon^p(\mathbf{x})$. As a result, $\Pi_{\mathcal{B}_\epsilon^p(\mathbf{x})}$ will project $\alpha \mathbf{v}_k$ onto a point on the boundary of the ϵ -ball, which is precisely the set $\{\mathbf{v} : \|\mathbf{v}\|_p = \epsilon\}$. Hence, $\lim_{\alpha \rightarrow \infty} \Pi_{\mathcal{B}_\epsilon^p(\mathbf{x})}(\mathbf{x}_{k-1} + \alpha \mathbf{v}_k) = \mathbf{x} + \lim_{\alpha \rightarrow \infty} \Pi_{\{\|\cdot\|_p=\epsilon\}}(\alpha \mathbf{v}_k)$. \square

Next we provide another very intuitive yet surprisingly hard⁸ to prove result:

Lemma 3 (Min-max-commutativity). *The order of the elementwise max and min in the projection (clipping) operator $\Pi_{\mathcal{B}_\epsilon^\infty(\mathbf{x})}$ can be exchanged, i.e.*

$$\max(-\epsilon, \min(\epsilon, \mathbf{x})) = \min(\epsilon, \max(-\epsilon, \mathbf{x})) \quad (90)$$

Proof. We are using the following representations which hold *elementwise* for all $\mathbf{a}, \mathbf{x} \in \mathbb{R}^n$:

$$\max(\mathbf{a}, \mathbf{x}) = \mathbf{a} + \max(0, \mathbf{x} - \mathbf{a}) = \mathbf{a} + \mathbb{1}_{\{\mathbf{a} < \mathbf{x}\}}(\mathbf{x} - \mathbf{a}) \quad (91)$$

$$\min(\mathbf{a}, \mathbf{x}) = \mathbf{a} + \min(0, \mathbf{x} - \mathbf{a}) = \mathbf{a} + \mathbb{1}_{\{\mathbf{x} < \mathbf{a}\}}(\mathbf{x} - \mathbf{a}) \quad (92)$$

where $\mathbb{1}_{\{\cdot\}}$ denotes the elementwise indicator function.

With these, we have

$$\max(-\epsilon, \min(\epsilon, \mathbf{x})) \quad (93)$$

$$= -\epsilon + \mathbb{1}_{\{-\epsilon < \min(\epsilon, \mathbf{x})\}}(\min(\epsilon, \mathbf{x}) + \epsilon) \quad (94)$$

$$= -\epsilon + \mathbb{1}_{\{-\epsilon < \mathbf{x}\}}(2\epsilon + \mathbb{1}_{\{\mathbf{x} < \epsilon\}}(\mathbf{x} - \epsilon)) \quad (95)$$

$$= -\epsilon + 2\epsilon \mathbb{1}_{\{-\epsilon < \mathbf{x}\}} + \mathbb{1}_{\{-\epsilon < \mathbf{x} < \epsilon\}}(\mathbf{x} - \epsilon) \quad (96)$$

$$= -\epsilon + 2\epsilon(\mathbb{1}_{\{-\epsilon < \mathbf{x} < \epsilon\}} + \mathbb{1}_{\{\epsilon < \mathbf{x}\}}) \\ + \mathbb{1}_{\{-\epsilon < \mathbf{x} < \epsilon\}}(\mathbf{x} - \epsilon) \quad (97)$$

$$= -\epsilon + 2\epsilon \mathbb{1}_{\{\epsilon < \mathbf{x}\}} + \mathbb{1}_{\{-\epsilon < \mathbf{x} < \epsilon\}}(\mathbf{x} + \epsilon) \quad (98)$$

$$= -\epsilon + 2\epsilon(1 - \mathbb{1}_{\{\mathbf{x} < \epsilon\}}) + \mathbb{1}_{\{-\epsilon < \mathbf{x} < \epsilon\}}(\mathbf{x} + \epsilon) \quad (99)$$

$$= \epsilon + \mathbb{1}_{\{\mathbf{x} < \epsilon\}}(-2\epsilon + \mathbb{1}_{\{-\epsilon < \mathbf{x}\}}(\mathbf{x} + \epsilon)) \quad (100)$$

$$= \epsilon + \mathbb{1}_{\{\max(-\epsilon, \mathbf{x}) < \epsilon\}}(\max(-\epsilon, \mathbf{x}) - \epsilon) \quad (101)$$

$$= \min(\epsilon, \max(-\epsilon, \mathbf{x})) \quad (102)$$

where we used that $\mathbb{1}_{\{-\epsilon < \min(\epsilon, \mathbf{x})\}} = \mathbb{1}_{\{-\epsilon < \mathbf{x}\}}$ and $\mathbb{1}_{\{\max(-\epsilon, \mathbf{x}) < \epsilon\}} = \mathbb{1}_{\{\mathbf{x} < \epsilon\}}$. \square

⁸The proof is easier yet less elegant if one alternatively resorts to case distinctions.

7.4. Proof of Main Theorem

Theorem 1 For ϵ small enough such that $\mathcal{B}_\epsilon^p(\mathbf{x}) \subset X(\phi_{\mathbf{x}})$ and in the limit $\alpha \rightarrow \infty$, ℓ_p -norm constrained projected gradient ascent based adversarial training with an ℓ_q -norm loss on the logits of the clean and perturbed input $\ell_{\text{adv}}(f(\mathbf{x}), f(\mathbf{x}^*)) = \|f(\mathbf{x}) - f(\mathbf{x}^*)\|_q$, with $p, q \in \{1, 2, \infty\}$, is equivalent to the power method limit of data-dependent (p, q) -operator norm regularization of the Jacobian $\mathbf{J}_f(\mathbf{x})$ of the network.

To prove the theorem we need to show that the updates for ℓ_p -norm constrained projected gradient ascent based adversarial training with an ℓ_q -norm loss on the logits in Equation 24 reduce to the corresponding updates for data-dependent operator norm regularization in Equation 16 under the above conditions on ϵ and α .

Proof. For an ℓ_q -norm loss on the logits of the clean and perturbed input $\ell_{\text{adv}}(f(\mathbf{x}), f(\mathbf{x}^*)) = \|f(\mathbf{x}) - f(\mathbf{x}^*)\|_q$, the corresponding ℓ_p -norm constrained projected gradient ascent updates in Equation 24 are

$$\begin{aligned} \mathbf{u}_k &\leftarrow \frac{\text{sign}(\tilde{\mathbf{u}}_k) \odot |\tilde{\mathbf{u}}_k|^{q-1}}{\|\tilde{\mathbf{u}}_k\|_q^{q-1}}, \quad \tilde{\mathbf{u}}_k \leftarrow f(\mathbf{x}_{k-1}) - f(\mathbf{x}) \\ \mathbf{v}_k &\leftarrow \frac{\text{sign}(\tilde{\mathbf{v}}_k) \odot |\tilde{\mathbf{v}}_k|^{p^*-1}}{\|\tilde{\mathbf{v}}_k\|_{p^*}^{p^*-1}}, \quad \tilde{\mathbf{v}}_k \leftarrow \mathbf{J}_f(\mathbf{x}_{k-1})^\top \mathbf{u}_k \\ \mathbf{x}_k &\leftarrow \Pi_{\mathcal{B}_\epsilon^p(\mathbf{x})}(\mathbf{x}_{k-1} + \alpha \mathbf{v}_k) \end{aligned} \quad (103)$$

In the limit $\alpha \rightarrow \infty$, $\mathbf{x}_{k-1} = \mathbf{x} + \epsilon \mathbf{v}_{k-1}$ by the ‘‘Projection Lemma’’ (Lemma 2) and thus for small enough ϵ , $f(\mathbf{x}_{k-1}) - f(\mathbf{x}) = \mathbf{J}_f(\mathbf{x})(\mathbf{x}_{k-1} - \mathbf{x}) = \epsilon \mathbf{J}_f(\mathbf{x}) \mathbf{v}_{k-1}$ (equality holds because $\mathbf{x}_{k-1} \in \mathcal{B}_\epsilon^p(\mathbf{x}) \subset X(\phi_{\mathbf{x}})$). Thus, the forward pass becomes

$$\mathbf{u}_k \leftarrow \frac{\text{sign}(\tilde{\mathbf{u}}_k) \odot |\tilde{\mathbf{u}}_k|^{q-1}}{\|\tilde{\mathbf{u}}_k\|_q^{q-1}}, \quad \tilde{\mathbf{u}}_k \leftarrow \mathbf{J}_f(\mathbf{x}) \mathbf{v}_{k-1} \quad (104)$$

For the backward pass, we have

$$\tilde{\mathbf{v}}_k = \mathbf{J}_f(\mathbf{x}_{k-1})^\top \mathbf{u}_k = \mathbf{J}_f(\mathbf{x})^\top \mathbf{u}_k, \quad (105)$$

since $\mathbf{J}_f(\mathbf{x}_k) = \mathbf{J}_f(\mathbf{x})$ for all $\mathbf{x}_k \in \mathcal{B}_\epsilon^p(\mathbf{x}) \subset X(\phi_{\mathbf{x}})$. Note that the update equation for \mathbf{x}_k is not needed since the Jacobians in the forward and backward passes don’t depend on \mathbf{x}_k , since $\mathbf{J}_f(\mathbf{x}_k) = \mathbf{J}_f(\mathbf{x})$ for all $\mathbf{x}_k \in \mathcal{B}_\epsilon^p(\mathbf{x}) \subset X(\phi_{\mathbf{x}})$. The update equations for ℓ_p -norm constrained projected gradient ascent based adversarial training with an ℓ_q -norm loss on the logits can therefore be written as

$$\begin{aligned} \mathbf{u}_k &\leftarrow \text{sign}(\tilde{\mathbf{u}}_k) \odot |\tilde{\mathbf{u}}_k|^{q-1} / \|\tilde{\mathbf{u}}_k\|_q^{q-1}, \quad \tilde{\mathbf{u}}_k \leftarrow \mathbf{J}_f(\mathbf{x}) \mathbf{v}_{k-1} \\ \mathbf{v}_k &\leftarrow \text{sign}(\tilde{\mathbf{v}}_k) \odot |\tilde{\mathbf{v}}_k|^{p^*-1} / \|\tilde{\mathbf{v}}_k\|_{p^*}^{p^*-1}, \quad \tilde{\mathbf{v}}_k \leftarrow \mathbf{J}_f(\mathbf{x})^\top \mathbf{u}_k \end{aligned} \quad (106)$$

which is precisely the power method limit of (p, q) operator norm regularization in Equation 16. We have thus shown

that the update equations to compute the adversarial perturbation and the data-dependent operator norm maximizer are exactly the same.

It is also easy to see that the objective functions used to update the network parameters for ℓ_p -norm constrained projected gradient ascent based adversarial training with an ℓ_q -norm loss on the logits of clean and adversarial inputs in Equation 18

$$\mathbf{E}_{(\mathbf{x}, y) \sim \hat{P}} \left[\ell(y, f(\mathbf{x})) + \lambda \max_{\mathbf{x}^* \in \mathcal{B}_\epsilon^p(\mathbf{x})} \|f(\mathbf{x}) - f(\mathbf{x}^*)\|_q \right] \quad (107)$$

is by the condition $\mathcal{B}_\epsilon^p(\mathbf{x}) \subset X(\phi_{\mathbf{x}})$ and $\mathbf{x}^* = \mathbf{x} + \epsilon \mathbf{v}$

$$\mathbf{E}_{(\mathbf{x}, y) \sim \hat{P}} \left[\ell(y, f(\mathbf{x})) + \lambda \epsilon \max_{\mathbf{v}^*: \|\mathbf{v}^*\|_p \leq 1} \|\mathbf{J}_f(\mathbf{x}) \mathbf{v}\|_q \right] \quad (108)$$

the same as that of data-dependent (p, q) operator norm regularization in Equation 17. \square

7.5. Gradient of p-Norm

The gradient of any p-norm is given by

$$\nabla_{\mathbf{x}} \|\mathbf{x}\|_p = \frac{\text{sign}(\mathbf{x}) \odot |\mathbf{x}|^{p-1}}{\|\mathbf{x}\|_p^{p-1}} \quad (109)$$

where \odot , $\text{sign}(\cdot)$ and $|\cdot|$ denote elementwise product, sign and absolute value.

In this section, we take a closer look at the $p \rightarrow \infty$ limit,

$$\lim_{p \rightarrow \infty} \nabla_{\mathbf{x}} \|\mathbf{x}\|_p = \frac{1}{|\mathcal{I}|} \text{sign}(\mathbf{x}) \odot \mathbf{1}_{\mathcal{I}} \quad (110)$$

with $\mathbf{1}_{\mathcal{I}} = \sum_{i \in \mathcal{I}} \mathbf{e}_i$, where $\mathcal{I} := \{j \in [1, \dots, n] : |x_j| = \|\mathbf{x}\|_\infty\}$ denotes the set of indices at which \mathbf{x} attains its maximum norm and \mathbf{e}_i is the i -th canonical unit vector.

The derivation goes as follows. Consider

$$\lim_{p \rightarrow \infty} \sum_i \frac{|x_i|^p}{\|\mathbf{x}\|_\infty^p} = \lim_{p \rightarrow \infty} \sum_i \left(\frac{|x_i|}{\|\mathbf{x}\|_\infty} \right)^p = |\mathcal{I}| \quad (111)$$

Thus

$$\frac{\|\mathbf{x}\|_p^{p-1}}{\|\mathbf{x}\|_\infty^{p-1}} = \left(\frac{\sum_i |x_i|^p}{\|\mathbf{x}\|_\infty^p} \right)^{(p-1)/p} \xrightarrow{p \rightarrow \infty} |\mathcal{I}| \quad (112)$$

since $|\mathcal{I}|^{(p-1)/p} \xrightarrow{p \rightarrow \infty} |\mathcal{I}|$. Now consider

$$\frac{\text{sign}(x_i) |x_i|^{p-1}}{\|\mathbf{x}\|_p^{p-1}} = \frac{\text{sign}(x_i) |x_i|^{p-1} / \|\mathbf{x}\|_\infty^{p-1}}{\|\mathbf{x}\|_p^{p-1} / \|\mathbf{x}\|_\infty^{p-1}} \quad (113)$$

The numerator

$$\text{sign}(x_i)|x_i|^{p-1}/\|\mathbf{x}\|_\infty^{p-1} \xrightarrow{p \rightarrow \infty} \begin{cases} 0 & \text{if } i \notin \mathcal{I} \\ \text{sign}(x_i) & \text{if } i \in \mathcal{I} \end{cases} \quad (114)$$

The denominator $\|\mathbf{x}\|_p^{p-1}/\|\mathbf{x}\|_\infty^{p-1} \xrightarrow{p \rightarrow \infty} |\mathcal{I}|$. The rest is clever notation.

7.6. Cross-Entropy based Adversarial Loss Function

The adversarial loss function determines the logit-space direction \mathbf{u}_k of the directional derivative in the power method like formulation of adversarial training in Equation 23.

Let us consider this for the softmax cross-entropy loss, defined as $\ell_{\text{adv}}(y, \mathbf{z}) := -\log(s_y(\mathbf{z}))$,

$$\ell_{\text{adv}}(y, \mathbf{z}) = -\mathbf{z}_y + \log\left(\sum_{k=1}^d \exp(\mathbf{z}_k)\right) \quad (115)$$

where the softmax is given by

$$s_y(\mathbf{z}) := \frac{\exp(\mathbf{z}_y)}{\sum_{k=1}^d \exp(\mathbf{z}_k)} \quad (116)$$

Untargeted ℓ_2 -PGA (forward pass)

$$\left[\tilde{\mathbf{u}}_k \leftarrow \nabla_{\mathbf{z}} \ell_{\text{adv}}(y, \mathbf{z}) \Big|_{\mathbf{z}=f(\mathbf{x}_k)} \right]_i = s_i(f(\mathbf{x}_k)) - \delta_{iy} \quad (117)$$

Targeted ℓ_2 -PGA (forward pass)

$$\left[\tilde{\mathbf{u}}_k \leftarrow -\nabla_{\mathbf{z}} \ell_{\text{adv}}(y_{\text{adv}}, \mathbf{z}) \Big|_{\mathbf{z}=f(\mathbf{x}_k)} \right]_i = \delta_{iy_{\text{adv}}} - s_i(f(\mathbf{x}_k)) \quad (118)$$

Notice that the logit gradient can be computed in a forward pass by analytically expressing it in terms of the arguments of the objective function.

Interestingly, for a temperature-dependent softmax cross-entropy loss, the logit-space direction becomes a ‘‘label-flip’’ vector in the low-temperature limit (high inverse temperature $\beta \rightarrow \infty$) where the softmax $s_y^\beta(\mathbf{z}) := \exp(\beta \mathbf{z}_y) / (\sum_{k=1}^d \exp(\beta \mathbf{z}_k))$ converges to the argmax: $s^\beta(\mathbf{z}) \xrightarrow{\beta \rightarrow \infty} \arg \max(\mathbf{z})$. E.g. for targeted attacks $\left[\tilde{\mathbf{u}}_k^{\beta \rightarrow \infty} \right]_i = \delta_{iy_{\text{adv}}} - \delta_{iy(\mathbf{x}_k)}$. This implies that in the high β limit, iterative PGA finds an input space perturbation \mathbf{v}_k that corresponds to the steepest ascent of f along the ‘‘label flip’’ direction $\mathbf{u}_k^{\beta \rightarrow \infty}$.

A note on canonical link functions. Interestingly, the gradient of the loss w.r.t. the logits of the classifier takes the form ‘‘prediction - target’’ for both the sum-of-squares error as well as the softmax cross-entropy loss. This is in fact a general result of modelling the target variable with a conditional distribution from the exponential family along with a canonical activation function. This means that adversarial attacks try to find perturbations in input space that induce a logit perturbation that aligns with the difference between the current prediction and the attack target.

7.7. Extracting Jacobian as a Matrix

Since we know that any neural network with its nonlinear activation function set to fixed values represents a linear operator, which, locally, is a good approximation to the neural network itself, we develop a method to fully extract and specify this linear operator in the neighborhood of any input datapoint \mathbf{x} . We have found the naive way of determining each entry of the linear operator by consecutively computing changes to individual basis vectors to be numerically unstable and therefore have settled for a more robust alternative:

In a first step, we run a set of randomly perturbed versions of \mathbf{x} through the network (with fixed activation functions) and record their outputs at the particular layer that is of interest to us (usually the logit layer). In a second step, we compute a linear regression on these input-output pairs to obtain a weight matrix \mathbf{W} as well as a bias vector \mathbf{b} , thereby fully specifying the linear operator. The singular vectors and values of \mathbf{W} can be obtained by performing an SVD.

7.8. Dataset, Architecture & Training Methods

We trained Convolutional Neural Networks (CNNs) with seven hidden layers and batch normalization on the CIFAR10 data set (Krizhevsky & Hinton, 2009). The CIFAR10 dataset consists of 60k 32×32 colour images in 10 classes, with 6k images per class. It comes in a pre-packaged train-test split, with 50k training images and 10k test images, and can readily be downloaded from <https://www.cs.toronto.edu/~kriz/cifar.html>.

We conduct our experiments on a pre-trained standard convolutional neural network, employing 7 convolutional layers, augmented with BatchNorm, ReLU nonlinearities and MaxPooling. The network achieves 93.5% accuracy on a clean test set. Relevant links to download the pre-trained model can be found in our codebase. For the robustness experiments, we also train a state-of-the-art Wide Residual Network (WRN-28-10) (Zagoruyko & Komodakis, 2016). The network achieves 96.3% accuracy on a clean test set.

We adopt the following standard preprocessing and data augmentation scheme: Each training image is zero-padded with four pixels on each side, randomly cropped to produce a new image with the original dimensions and horizontally flipped with probability one half. We also standardize each image to have zero mean and unit variance when passing it to the classifier.

The attack strength ϵ used for PGA was chosen to be the smallest value such that almost all adversarially perturbed inputs to the standard model are successfully misclassified, which is $\epsilon = 1.75$. The regularization constants of the other training methods were then chosen in such a way that they roughly achieve the same test set accuracy on clean exam-

Table 3. CIFAR10 test set accuracies and hyper-parameters for the models and training methods we considered. The regularization constants were chosen such that the models achieve roughly the same accuracy on clean test examples as the adversarially trained model does. See Table 4 for the full hyper-parameter sweep.

MODEL & TRAINING METHOD	ACC	HYPER-PARAMETERS
<i>CNN7</i>		
STANDARD TRAINING	93.5%	—
ADVERSARIAL TRAINING	83.6%	$\epsilon = 1.75, \alpha = 2\epsilon/\text{ITERS}, \text{ITERS} = 10$
GLOBAL SPECTRAL NORM	80.4%	$\lambda = 3 \cdot 10^{-4}, \text{ITERS}=1, (10, \text{APPENDIX})$
DATA-DEP. SPECTRAL NORM	84.6%	$\lambda = 3 \cdot 10^{-2}, \epsilon = 1.75, \text{ITERS} = 10$
<i>WRN-28-10</i>		
STANDARD TRAINING	96.3%	—
ADVERSARIAL TRAINING	91.8%	$\epsilon = 1.75, \alpha = 2\epsilon/\text{ITERS}, \text{ITERS} = 10$
DATA-DEP. SPECTRAL NORM	91.3%	$\lambda = 3 \cdot 10^{-1}, \epsilon = 1.75, \text{ITERS} = 10$

ples as the adversarially trained model does, i.e. we allow a comparable drop in clean accuracy for regularized and adversarially trained models. When training the derived regularized models, we started from a pre-trained checkpoint and ran a hyper-parameter search over number of epochs, learning rate and regularization constants. Table 3 summarizes the test set accuracies and hyper-parameters for all the training methods we considered.

7.9. Hyperparameter Sweep

Table 4 details the hyperparameter configurations we searched during training. Table 3 shows the final set of hyperparameters for the best performing models.

7.10. Adversarial Training with Large α

Figure 6 shows the result of empirically raising the adversarial learning rate during adversarial training with PGA to very large values. As can be seen, the adversarial robustness initially rises, but after some threshold it levels out and does not change significantly even at very large values.

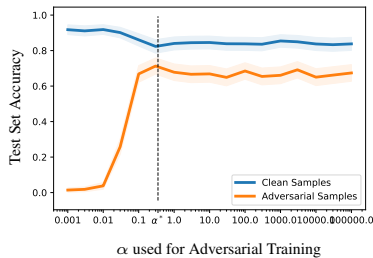


Figure 6. Test set accuracy on clean and adversarial examples after using adversarial (PGA) training with a given step size α . The dashed line indicates the α used when generating adversarial examples at test time. The ϵ in the projection was fixed to the value used in the main text.

7.11. Alignment of Adversarial Perturbations with Dominant Singular Vector

Figure 7 shows the cosine-similarity of adversarial perturbations of magnitude ϵ with the dominant singular vector of $\mathbf{J}_f(\mathbf{x})$, as a function of perturbation magnitude ϵ . For comparison, we also include the alignment with random perturbations. For all training methods, the larger the perturbation magnitude ϵ , the lesser the adversarial perturbation aligns with the dominant singular vector of $\mathbf{J}_f(\mathbf{x})$, which is to be expected for a simultaneously increasing deviation from linearity. The alignment is similar for adversarially trained and data-dependent spectral norm regularized models and for both larger than that of global spectral norm regularized and naturally trained models.

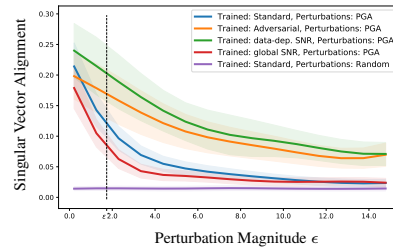


Figure 7. Alignment of adversarial perturbations with dominant singular vector of $\mathbf{J}_f(\mathbf{x})$ as a function of perturbation magnitude ϵ . The dashed vertical line indicates the ϵ used during adversarial training. Curves were aggregated over 2000 test samples.

7.12. Activation Patterns

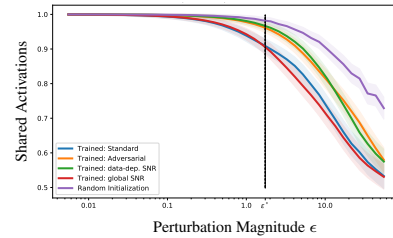


Figure 8. Fraction of shared activations as a function of perturbation magnitude ϵ between activation patterns $\phi_{\mathbf{x}}$ and $\phi_{\mathbf{x}^*}$, where \mathbf{x} is a data point sampled from the test set, and \mathbf{x}^* is an adversarially perturbed input, with perturbation magnitude ϵ .

7.13. Further Experimental Results for global SNR with 10 iterations

In the main section, we have implemented the baseline version of global SNR as close as possible to the descriptions in (Yoshida & Miyato, 2017). However, this included a recommendation from the authors to perform only a single update iteration to the spectral decompositions of the weight matrices per training step. As this is computationally less demanding than the 10 iterations per training step spent on

Table 4. Hyperparameter sweep during training. We report results for the best performing models in the main text.

TRAINING METHOD	HYPERPARAMETER	VALUES TESTED
ADVERSARIAL TRAINING	ϵ	0.5, 0.75, 1.0, 1.25, 1.5, 1.75, 2.0, 2.25, 2.5, 2.75, 3.0, 3.25, 3.5, 3.75, 4.0
	α	ϵ/ITERS , $2\epsilon/\text{ITERS}$, $3\epsilon/\text{ITERS}$, $4\epsilon/\text{ITERS}$, $5\epsilon/\text{ITERS}$
	ITERS	1, 2, 3, 5, 8, 10, 15, 20, 30, 40, 50
GLOBAL SPECTRAL NORM REG.	λ	$1 \cdot 10^{-5}$, $3 \cdot 10^{-5}$, $1 \cdot 10^{-4}$, $3 \cdot 10^{-4}$, $1 \cdot 10^{-3}$, $3 \cdot 10^{-3}$, $1 \cdot 10^{-2}$, $3 \cdot 10^{-2}$, $1 \cdot 10^{-1}$, $3 \cdot 10^{-1}$, $1 \cdot 10^0$, $3 \cdot 10^0$, $1 \cdot 10^1$, $3 \cdot 10^1$
	ITERS	1, 10
DATA-DEP. SPECTRAL NORM REG.	λ	$1 \cdot 10^{-5}$, $3 \cdot 10^{-5}$, $1 \cdot 10^{-4}$, $3 \cdot 10^{-4}$, $1 \cdot 10^{-3}$, $3 \cdot 10^{-3}$, $1 \cdot 10^{-2}$, $3 \cdot 10^{-2}$, $1 \cdot 10^{-1}$, $3 \cdot 10^{-1}$, $1 \cdot 10^0$, $3 \cdot 10^0$, $1 \cdot 10^1$, $3 \cdot 10^1$
	ITERS	1, 2, 3, 5, 8, 10, 15, 20, 30, 40, 50

both adversarial training, as well as data-dependent spectral norm regularization, we verify that performing 10 iterations makes no difference to the method of (Yoshida & Miyato, 2017). Figures 9 and 10 reproduce the curves for global SNR from the main part (having used 1 iteration) and overlap it with the same experiments, but done with global SNR using 10 iterations. As can be seen, there is no significant difference between the two.

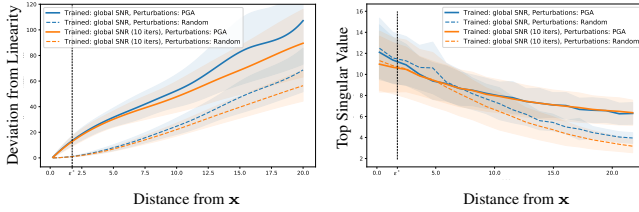


Figure 9. (Left) Deviation from linearity $\|\phi^{L-1}(\mathbf{x} + \mathbf{z}) - (\phi^{L-1}(\mathbf{x}) + \mathbf{J}_{\phi^{L-1}}(\mathbf{x})\mathbf{z})\|_2$ as a function of the distance $\|\mathbf{z}\|_2$ from \mathbf{x} for random and adversarial perturbations \mathbf{z} . (Right) Largest singular value of the linear operator $\mathbf{J}_f(\mathbf{x} + \mathbf{z})$ as a function of the magnitude $\|\mathbf{z}\|_2$ of random and adversarial perturbations \mathbf{z} . The dashed vertical line indicates the ϵ used during adversarial training. Curves were aggregated over 200 samples from the test set.

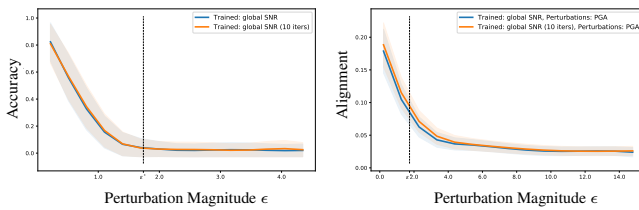


Figure 10. (Left) Classification accuracy as a function of perturbation strength ϵ . (Right) Alignment of adversarial perturbations with dominant singular vector of $\mathbf{J}_f(\mathbf{x})$ as a function of perturbation magnitude ϵ . The dashed vertical line indicates the ϵ used during adversarial training. Curves were aggregated over 2000 samples from the test set.

7.14. Further Experimental Results for ℓ_∞ -norm Constrained Projected Gradient Ascent

Additional results against ℓ_∞ -norm constrained PGA attacks are provided in Figures 11 & 12. The conclusions remain the same for all the experiments we conducted.

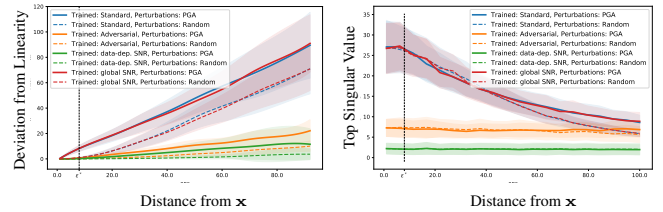


Figure 11. (Left) Deviation from linearity $\|\phi^{L-1}(\mathbf{x} + \mathbf{z}) - (\phi^{L-1}(\mathbf{x}) + \mathbf{J}_{\phi^{L-1}}(\mathbf{x})\mathbf{z})\|_2$ as a function of the distance $\|\mathbf{z}\|_2$ from \mathbf{x} for random and ℓ_∞ -PGA adversarial perturbations \mathbf{z} . (Right) Largest singular value of $\mathbf{J}_{\phi^{L-1}}(\mathbf{x} + \mathbf{z})$ as a function of the magnitude $\|\mathbf{z}\|_2$ of random and ℓ_∞ -PGA adversarial perturbations \mathbf{z} . The dashed vertical line indicates the ϵ used during adversarial training. Curves were aggregated over 200 test samples.

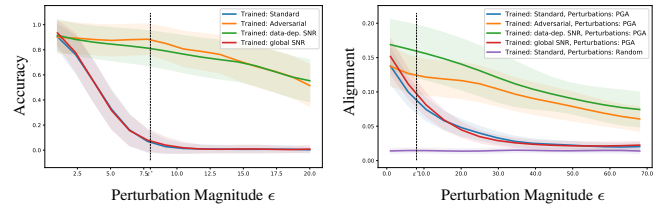


Figure 12. (Left) Classification accuracy as a function of perturbation strength ϵ (measured in 8-bit). (Right) Alignment of ℓ_∞ -PGA adversarial perturbations with dominant singular vector of $\mathbf{J}_f(\mathbf{x})$ as a function of perturbation magnitude ϵ . The dashed vertical line indicates the ϵ used during adversarial training. Curves were aggregated over 2000 samples from the test set.